

Quasi-Analytic Models for Density Bubbles and Plasma Clouds in the Equatorial Ionosphere

Paul A. Bernhardt

Plasma Physics Division, Naval Research Laboratory
Washington, DC 20375
USA

bern@ppd.nrl.navy.mil

ABSTRACT

The equatorial ionosphere contains imbedded bubbles that rise through a horizontally stratified plasma. The motion of the bubbles are affected by gravity, neutral winds or external electric fields which produce electric fields in the F-Region density perturbations of the bubbles. Exact solutions for the electric potentials are derived assuming linear or circular symmetry to the density structures imbedded in the background plasma. A wide variety of analytic solutions for electric potentials are found for both density cavities and density enhancements. An analytic description of a rising bubble can be constructed by attaching a tail to the top half of a circular hole to form the electron density solution. The potential for this plume structure is a weighted sum of the analytic solutions for each separate piece. Using this electric potential, quasi-analytic solutions for the transport of the bubbles are derived using the continuity equation for the plasma with production and loss terms neglected. The analytic models of the electric fields provide incompressible motion that transports the locations of "plasma cells" but does not change the density of the plasma in each cell. This Lagrangian approach employs a time dependent coordinate mapping of the undisturbed layer grid. Using internal electric potentials of the bubbles and external polarizations of the F-layer as a whole, a transport model yields tilted plasma plumes that move through the F-Region. This time-dependent computer model provides useful plasma densities in a fraction of the time for fully numerical simulations.

1.0 INTRODUCTION

The F-Region ionosphere can become unstable if a density perturbation becomes electrically polarized by external forces from electric fields, neutral winds, and gravitational acceleration. Near the geomagnetic equator, gravity can act on the plasma attached to the nearly horizontal magnetic field lines to produce unstable conditions. After sunset when the layer is lifted by ambient electric fields, the bottom-side steepens and plasma bubbles are formed. These bubbles rise through the layer in response to a Rayleigh-Taylor type instability. Also, winds or electric fields induce electric fields in both density cavities and enhancements that cause distortions in the density structures. These distorted plasma structures are responsible for degradation of radio propagation that lead to navigation errors and outages, communications systems failures and radar clutter. The modeling of ionospheric bubbles or density enhancements uses computer simulations that calculate the effects of self-generated electric fields (E) that are driven by gravity, neutral winds and external electric fields. Numerical computation of the electric potentials requires the most time and effort in the bubble modeling process. The electric fields for these simulations can be found numerically using direct or iterative solvers of the non-separable potential equations that describe the self-generated electric fields (e.g.

Bernhardt, P.A. (2006) Quasi-Analytic Models for Density Bubbles and Plasma Clouds in the Equatorial Ionosphere. In *Characterising the Ionosphere* (pp. 18-1 – 18-46). Meeting Proceedings RTO-MP-IST-056, Paper 18. Neuilly-sur-Seine, France: RTO. Available from: <http://www.rto.nato.int/abstracts.asp>.

Report Documentation Page				Form Approved OMB No. 0704-0188	
Public reporting burden for the collection of information is estimated to average 1 hour per response, including the time for reviewing instructions, searching existing data sources, gathering and maintaining the data needed, and completing and reviewing the collection of information. Send comments regarding this burden estimate or any other aspect of this collection of information, including suggestions for reducing this burden, to Washington Headquarters Services, Directorate for Information Operations and Reports, 1215 Jefferson Davis Highway, Suite 1204, Arlington VA 22202-4302. Respondents should be aware that notwithstanding any other provision of law, no person shall be subject to a penalty for failing to comply with a collection of information if it does not display a currently valid OMB control number.					
1. REPORT DATE 01 JUN 2006		2. REPORT TYPE N/A		3. DATES COVERED -	
4. TITLE AND SUBTITLE Quasi-Analytic Models for Density Bubbles and Plasma Clouds in the Equatorial Ionosphere				5a. CONTRACT NUMBER	
				5b. GRANT NUMBER	
				5c. PROGRAM ELEMENT NUMBER	
6. AUTHOR(S)				5d. PROJECT NUMBER	
				5e. TASK NUMBER	
				5f. WORK UNIT NUMBER	
7. PERFORMING ORGANIZATION NAME(S) AND ADDRESS(ES) Plasma Physics Division, Naval Research Laboratory Washington, DC 20375 USA				8. PERFORMING ORGANIZATION REPORT NUMBER	
9. SPONSORING/MONITORING AGENCY NAME(S) AND ADDRESS(ES)				10. SPONSOR/MONITOR'S ACRONYM(S)	
				11. SPONSOR/MONITOR'S REPORT NUMBER(S)	
12. DISTRIBUTION/AVAILABILITY STATEMENT Approved for public release, distribution unlimited					
13. SUPPLEMENTARY NOTES See also ADM002065., The original document contains color images.					
14. ABSTRACT					
15. SUBJECT TERMS					
16. SECURITY CLASSIFICATION OF:			17. LIMITATION OF ABSTRACT UU	18. NUMBER OF PAGES 46	19a. NAME OF RESPONSIBLE PERSON
a. REPORT unclassified	b. ABSTRACT unclassified	c. THIS PAGE unclassified			

Quasi-Analytic Models for Density Bubbles and Plasma Clouds in the Equatorial Ionosphere

[1]). The computational time for solving for the disturbed ionosphere is often prohibitive so analytic solutions to both the transport and potential equations are useful. Exact analytic solutions for the electric potential can be used to test the numerical algorithms and to determine errors produced by boundary conditions and numerical round-off. The analytic solutions also yield insight into the conditions for production of ionospheric bubbles.

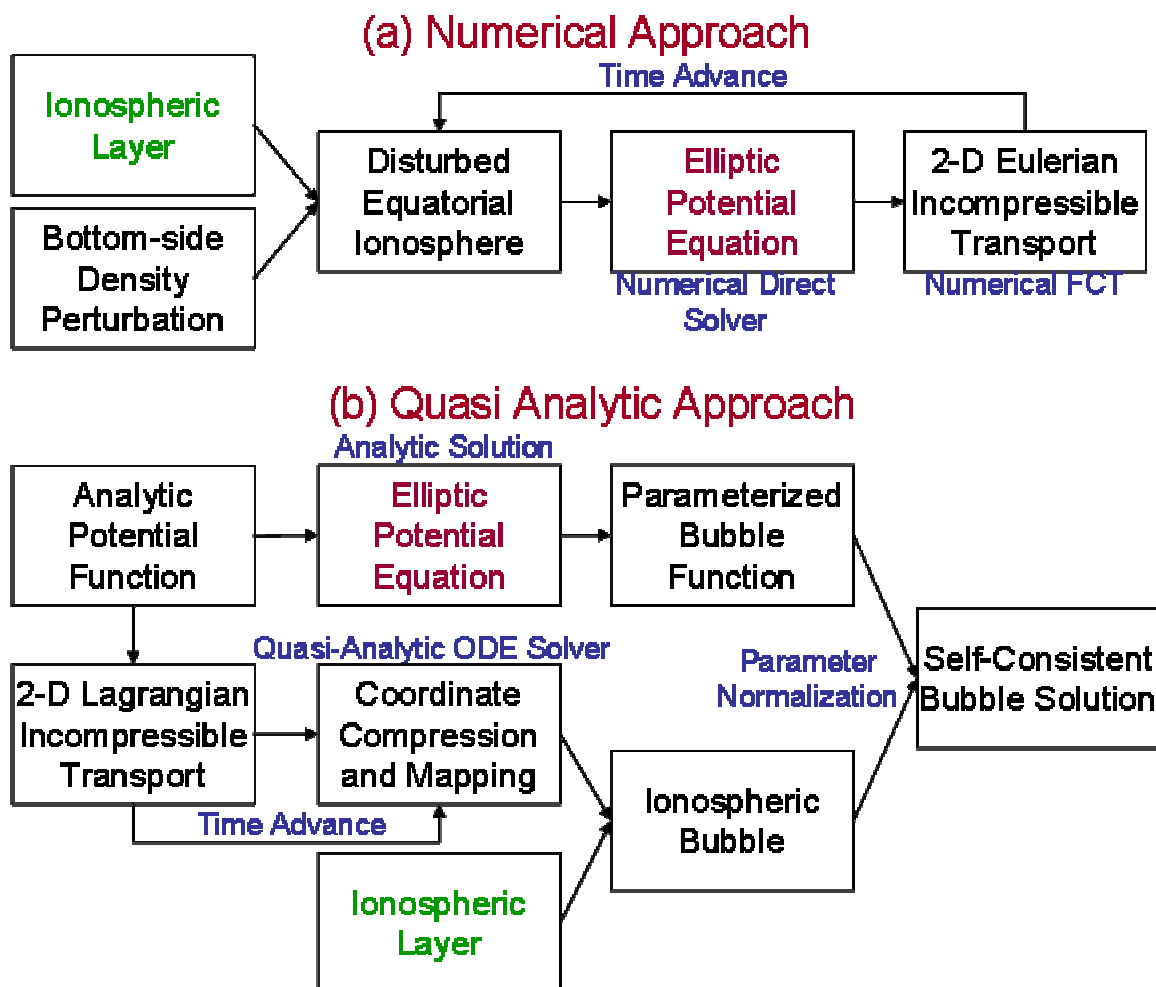


Figure 1: Block diagrams of (a) numerical and (b) quasi-analytic algorithms for ionospheric bubble modeling. Both approaches use an equivalent set of equations but apply different solution techniques and different frames of reference. This paper focuses on the solution of the elliptic potential shown in red for the (b) quasi-analytic approach.

The computational and analytical techniques for simulations of equatorial bubbles are compared in Figure 1. Typically, numerical models of equatorial bubbles follow the procedure illustrated by the block diagram given in Figure 1a. A stratified model of the F-layer is perturbed by a small density disturbance. Gravity is allowed to setup an electric potential in this plasma. The electric potential is obtained with a numerical solution of a non-separable elliptic equation using a direct solver such as described in Appendix A. Once the electric potential is obtained, the plasma transported in response to the electric fields for a small time step. A non-

dissipative flux corrected transport algorithm [9] is then used for incrementally move the plasma disturbance. The process is repeated with the generation of a revised electric potential followed by more incremental plasma transport. All of these processes are numerically intensive and can require several hours of computation.

A new approach for the quasi-analytic model of the equatorial bubble is proposed using the three steps in Figure 1b. First, the electric potential is defined by an analytic function that gives self-consistent expressions for electron density (or Pedersen conductivity) structures that are obtained in the presence of background electric fields, neutral winds and gravity. This procedure is described in the next section of this paper. Second, the plasma transport is determined using incompressible motion from the induced electric fields. The plasma transport is derived with the analytic electric potential distorting the coordinates with out changing the density in each coordinate cell. The third step is to adjust the parameters in the analytic models to that the analytic solution given in step 1 matches the quasi-analytic results from step 2. The application of the transport and normalization processes will be described in the later sections of this paper.

2.0 ANALYTIC MODELS FOR THE ELECTRIC POTENTIAL IN A DISTURBED IONOSPHERE

The equatorial ionosphere is commonly thought of as a uniform layer with the occasional imbedded structure or bubble. The modeling of ionospheric bubbles uses computer simulations that calculate the effects of self generated electric fields (\mathbf{E}) that are driven by gravity, neutral winds and external electric fields. The equations for these simulations can be found in a number of papers including [2]. For the analytic solutions considered here, the background ionosphere will be uniform in the horizontal, x- and z-directions. The ambient magnetic field, \mathbf{B} , is aligned with the z-axis. The altitude variations of the undisturbed ionosphere will be represented by the function $n_{e0}(y)$ where y is the vertical coordinate.

The layer becomes distorted when a small perturbation grows as electric fields provide incompressible perpendicular motion at F-region altitudes. These internal electric fields move plasma across magnetic field lines with the velocity

$$\mathbf{v} = \frac{\mathbf{E} \times \mathbf{B}}{B_0^2} = -\frac{\nabla\Phi \times \mathbf{B}}{B_0^2} \quad (1)$$

where \mathbf{v} is the velocity perpendicular to the ambient magnetic field \mathbf{B} and the electric field $\mathbf{E} = -\nabla\Phi$ can be represented as the gradient of a scalar electrostatic potential Φ . Other perpendicular components of velocity driven by pressure gradients, neutral winds, and gravity can be neglected because the plasma in the F-region ionosphere is magnetized. This means that the electron and ion gyro frequencies are much larger than the corresponding collision frequencies with the background neutral gas.

An analytic approach is derived to solve for the electric potential for localized electron density perturbations driven by external vector fields Kelley [6] gives the electric current in the F-region as

$$\mathbf{J} = [\mathbf{E} + \mathbf{E}_0 + (\mathbf{U} + \frac{\mathbf{g}}{v_{in}}) \times \mathbf{B}] \sigma_p \quad (2)$$

Quasi-Analytic Models for Density Bubbles and Plasma Clouds in the Equatorial Ionosphere

where $\sigma_p = \frac{e}{B_0} \frac{n_e v_{in}}{\Omega_i}$ is the Pedersen conductivity, $n_e(x, y, z)$ is the electron density, v_{in} is the ion neutral collisions frequency, \mathbf{E}_0 is the external electric field perpendicular to \mathbf{B} , $\mathbf{U} = U_x \tilde{\mathbf{x}} + U_y \tilde{\mathbf{y}}$ gives the normal components of the neutral wind vector, $\mathbf{g} = -g_0 \tilde{\mathbf{y}}$ is the gravitational acceleration, $\mathbf{B} = B_0 \tilde{\mathbf{z}}$ is the magnetic field vector and the inertial terms in the momentum equation have been neglected. Assume that the normal electric fields are constant along the magnetic field in the z -direction and that there is no z -component of current \mathbf{J} . For specific gravitational accelerations, neutral winds and external electric fields, the potential equation is found from (2) using

$$\frac{\partial J_z}{\partial z} + \nabla_{\perp} \cdot \mathbf{J} = 0 \quad (3)$$

Substitution of (2) into (3) and integration along the z -direction leaves an equation for the potential in the perpendicular (\perp) x - and y - directions.

$$\nabla_{\perp} \cdot (\Sigma_p \nabla_{\perp} \Phi) = \Sigma_p \nabla_{\perp}^2 \Phi + \nabla_{\perp} \Phi \cdot \nabla_{\perp} \Sigma_p = \nabla_{\perp} \cdot \int [\mathbf{E}_0 + (\mathbf{U} + \frac{\mathbf{g}}{v_{in}}) \times \mathbf{B}] \sigma_p dz \quad (4)$$

where $\Sigma_p = \int \sigma_p dz$ is the field-line-integrated Pedersen conductivity and $\mathbf{E} = -\nabla_{\perp} \Phi$ is the induced electric field. For simplicity, the driving fields \mathbf{E}_0 , \mathbf{U} , and $\frac{\mathbf{g}}{v_{in}}$ are assumed constant in space and time, then the potential equation simplifies to

$$\nabla_{\perp}^2 \Phi = \{[\mathbf{E}_0 + (\mathbf{U} + \frac{\mathbf{g}}{v_{in}}) \times \mathbf{B}] - \nabla_{\perp} \Phi\} \cdot \nabla_{\perp} \ln(\Sigma_p) = \{\mathbf{E}_T - \nabla_{\perp} \Phi\} \cdot \nabla_{\perp} \ln(\Sigma_p) \quad (5)$$

where the equivalent electric field vector defined by $\mathbf{E}_T \equiv \mathbf{E}_0 + (\mathbf{U} + \frac{\mathbf{g}}{v_{in}}) \times \mathbf{B}$. Given a spatial distribution for the Pedersen conductivity (or electron density), the potential is usually obtained numerically from the non-separable elliptic equation (5). Often iterative solvers requiring relatively long solution times or direct solvers requiring large memories are required to compute this solution.

A computational alternate approach assumes that the potential is given and (5) is used to find the associated electron density. For this solution, only Pedersen currents in the horizontal, x -direction will be considered so

$$[E_{0x} + (U_y - \frac{g_0}{v_{in}}) B_0] \tilde{\mathbf{x}} \equiv E_{Tx} \tilde{\mathbf{x}} \quad (6)$$

where E_{Tx} represents the equivalent driving fields from a static electric field in the positive x -direction, a neutral wind in the positive y -direction and gravitational acceleration along the positive y -axis. The sign of E_{Tx} is negative for the downward acceleration of gravity. In our notation, the growth rate for the Rayleigh-Taylor instability is $\gamma = (-E_{Tx}/B_0)/L_N$ where L_N is the scale length of the gradient on the bottom side of the ionosphere [8].

In normalized Cartesian coordinates, (4) becomes

$$\frac{\partial^2 \hat{\Phi}}{\partial \hat{x}^2} + \frac{\partial \text{Log}(\Sigma_p)}{\partial \hat{x}} \frac{\partial \hat{\Phi}}{\partial \hat{x}} + \frac{\partial^2 \hat{\Phi}}{\partial \hat{y}^2} + \frac{\partial \text{Log}(\Sigma_p)}{\partial \hat{y}} \frac{\partial \hat{\Phi}}{\partial \hat{y}} - \frac{\partial \text{Log}(\Sigma_p)}{\partial \hat{x}} = 0 \quad (7)$$

where often gravitational forcing is the sole contribution to E_{Tx} , $\hat{\Phi} = \frac{\Phi}{E_{Tx} r_0}$ is the dimensionless, normalized

potential, $(\hat{x}, \hat{y}) = \left(\frac{x}{r_0}, \frac{y}{r_0} \right)$ are the normalized coordinates, and r_0 is a constant scale factor for all distances.

Note that (7) has many self-similar elements. Multiplying the \hat{x} - and \hat{y} - coordinates as well as $\hat{\Phi}$ by a constant scale factor (i.e., r_0) does not change the equation. Multiplying Σ_p by a constant C_0 also yields a solution. Consequently, if $\hat{\Phi}(\hat{x}, \hat{y})$ and $\Sigma_p(\hat{x}, \hat{y})$ satisfies (7) then so do the pairs of functions $r_0 \hat{\Phi}(\frac{x}{r_0}, \frac{y}{r_0})$

and $C_0 \Sigma_p(\frac{x}{r_0}, \frac{y}{r_0})$. Normalized coordinates (\hat{x}, \hat{y}) will be used to simplify the notation for the analytic solutions.

The existence of analytic solutions for (7) was discovered by examining numerical solutions. A numerical algorithm for non-separable elliptic equations similar to (7) was written using a block tri-diagonal solver of the algebraic equation derived from finite difference approximations to the partial derivatives (Appendix A).

When a circularly symmetric function, $\Sigma_p(\hat{r})$ where $\hat{r} = \sqrt{\hat{x}^2 + \hat{y}^2}$, was used for the Pedersen conductivity it was found that the integral of the resulting electric potential along \hat{x} was also circularly symmetric. In mathematical terms,

$$\Sigma_p(\hat{r}) \Rightarrow \int \Phi(\hat{x}, \hat{y}) d\hat{x} = F_1(\hat{r}) \quad (8)$$

This immediately shows that the form of the potential is the \hat{x} coordinate multiplied by a circularly symmetric function since

$$\Phi(\hat{x}, \hat{y}) = \frac{F_1(\hat{r})}{\partial \hat{x}} = \frac{F_1(\hat{r})}{\partial \hat{r}} \frac{\partial \hat{r}}{\partial \hat{x}} = \frac{F_1(\hat{r})}{\partial \hat{r}} \frac{\hat{x}}{\hat{r}} = F_2(\hat{r}) \hat{x} \quad (9)$$

Functions of single variables such as \hat{r} can be solved analytically.

General analytic solutions to (7) can be derived by making simplifying assumptions about the form of $\hat{\Phi}$ and $\text{Log}(\Sigma_p)$. Numerical simulations for symmetric perturbations in x with x -directed fields given by (6) yield electric potentials that are odd functions of x with the form

$$\hat{\Phi}(\hat{x}, \hat{y}) = (a_0 + a_1 \hat{x}) G[q(\hat{x}, \hat{y})] \quad (10)$$

where a_0 and a_1 are constants, $q(\hat{x}, \hat{y}) = \sqrt{\hat{x}^2 + s \hat{y}^2}$ is a single variable representing an elliptical perturbation for the potential and “s” determines the polarization of the coordinate ellipse.

Quasi-Analytic Models for Density Bubbles and Plasma Clouds in the Equatorial Ionosphere

The Pedersen conductivity (or electron density) takes the form of an elliptically shaped perturbation modulating the background conductivity.

$$\text{Log}[\Sigma_p^{(s)}(\bar{x}, \bar{y})] = L_p[q(\bar{x}, \bar{y}), s] + \log[\Sigma_{p0}(\bar{y})] \quad (11)$$

where $L_p(q, s)$ is the natural log of the conductivity/density perturbation and $\Sigma_{p0}(\bar{y}) = \int \frac{e}{B} \frac{n_{e0}(\bar{y}, \bar{z}) v_{in}}{\Omega_i} r_0 d\bar{z}$

is the integrated conductivity associated with the horizontally stratified plasma layer. The last term of the left side of (7) is x-direction gradient of the log-Pedersen conductivity which drives the solution for the potential. Consequently, the \bar{x} variation through the function q is required to obtain useful solutions for the potential.

Substitution of (10) and (11) into (7) and solving for the derivative of $L_p(q)$ yields the equation

$$L'_p(q, s) = - \frac{q^2 G'(q) \left\{ \frac{2a_1 \bar{x}}{a_0 + a_1 \bar{x}} + s + s\bar{y} \frac{\partial \log[\Sigma_{p0}(\bar{y})]}{\partial \bar{y}} \right\} + q^3 G''(q) + \bar{y}^2 (s-1) s [q G''(q) - G'(q)]}{\frac{\bar{x} q^2 [a_1 G(q) - 1]}{a_0 + a_1 \bar{x}} + q^3 G'(q) + \bar{y}^2 (s-1) s q G'(q)} \quad (12)$$

where the prime (') denotes the derivative with respect to q . If the functions of \bar{y} vanish, (12) may be integrated directly. The \bar{y}^2 terms vanish only if $s = 0$, or 1.

General solutions for an extended vertical plume imposed on a horizontally stratified ionosphere are considered first. For $s = 0$ the potential has no variations in the altitude coordinate (\bar{y}) and the solutions for (10) and (11) are given by

$$\begin{aligned} q &= |\bar{x}| \\ \hat{\Phi}^{(0)}(\bar{x}) &= (a_0 + a_1 \bar{x}) G(q) \\ L'_p(q, 0) &= - \frac{2 a_1 \bar{x} G'(q) + q (a_0 + a_1 \bar{x}) G''(q)}{\bar{x} [a_1 G(q) - 1] + q (a_0 + a_1 \bar{x}) G'(q)} \\ \Sigma_p^{(0)}(\bar{x}, \bar{y}) &= C_0 \Sigma_{p0}(\bar{y}) \frac{-1}{(a_0 + a_1 \bar{x}) G'(q) + a_1 G(q) - 1} \end{aligned} \quad (13)$$

where C_0 is a constant chosen to give the background conductivity as $\bar{x} \rightarrow \infty$. Exact solutions for pairs of Pedersen conductivity and electric potentials from (13) are easily found. Table I gives several examples these pairs.

Exact solutions for pairs of Pedersen conductivity and electric potentials from (13) are easily found. The last equation in (13) can be inverted to give

$$G(\bar{x}) = \frac{1}{(a_0 + a_1 \bar{x})} \int_0^{\bar{x}} [1 - \Sigma_p^{(0)}(q)^{-1}] dq \quad (14)$$

where $\Sigma_p^{(0)}(\bar{x}) = \frac{\Sigma_p^{(0)}(\bar{x}, \bar{y})}{C_0 \Sigma_{p0}(\bar{y})}$ is the normalized 1-dimensional density cross section in the horizontal direction.

From the second equation in (13), the electric potential is found as

$$\widehat{\Phi}^{(0)}(\bar{x}) = \int_0^{\bar{x}} [1 - \Sigma_p^{(0)}(q)^{-1}] dq \quad (15)$$

Table I. Electron Density Disturbances and Companion 1-D Potential Functions

Pedersen Conductivity Function, $\Sigma_p^{(0)}(\bar{x}, \bar{y})$	Electric Potential, $\widehat{\Phi}(\bar{x}, \bar{y})$
$\frac{\Sigma_{p0}(\bar{y}) \exp(b \bar{x}^2)}{\exp(b \bar{x}^2) + 2b(a_0 + a_1 \bar{x})\bar{x} - a_1}$	$(a_0 + a_1 \bar{x}) \exp(-b \bar{x}^2)$
$\frac{\Sigma_{p0}(\bar{y}) (1 + \bar{x} ^b)^2}{(1 + \bar{x} ^b)^2 + a_1(b-1) \bar{x} ^b - a_1}$	$\frac{a_1 \bar{x}}{1 + \bar{x} ^b}$
$\frac{\Sigma_{p0}(\bar{y}) \cosh[b \bar{x}]}{\cosh[b \bar{x}] - a_1 + b(a_0 + a_1 \bar{x}) \sinh[b \bar{x}]}$	$(a_0 + a_1 \bar{x}) \operatorname{sech}[b \bar{x}]$

An example of the second function in Table I is illustrated in Figure 2 with the parameters $a_1 = -0.5$ and $b = 3$. The conductivity trough (Figure 2a) centered along the y-axis has a ridges that increase in amplitude as the parameter “ a_1 ” is increased. If $a_1 > 0$, the trough is replaced by a Pedersen conductivity enhancement as the sense of the potential (Figure 2b) is reversed. The parameter “ b ” simultaneously controls the steepness of the walls on the conductivity irregularity and the spatial decay of the potential function. With separation of variables, even more general solutions to (7) can be found in Cartesian coordinates. The 1-D conductivity structure and electric potential represent the “tail” portion of an ionospheric bubble.

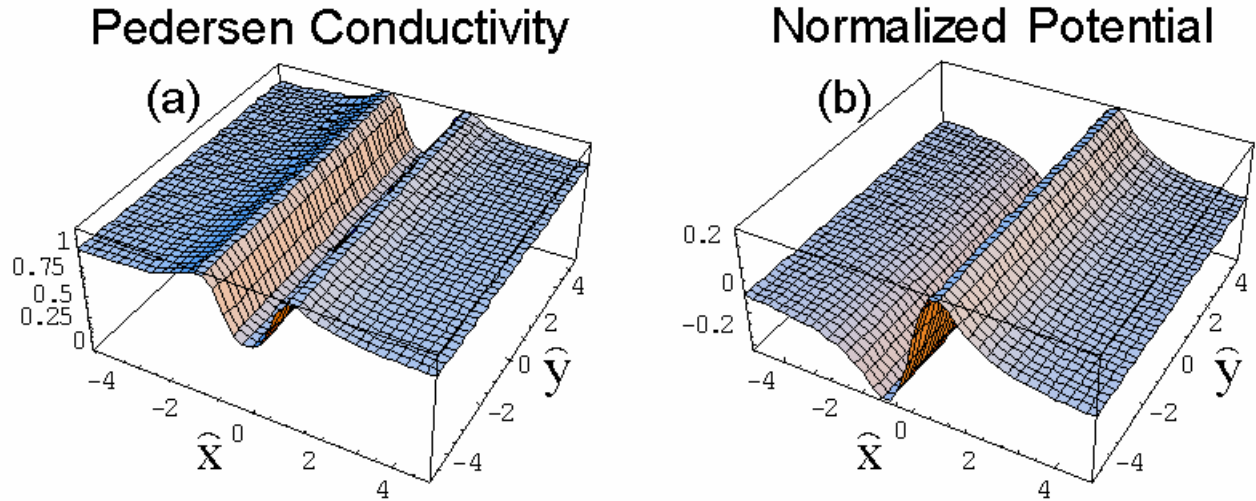


Figure 2. One-Dimensional Pedersen conductivity associated with the 1-D analytic electric potential using the parameters $a_1 = -0.5$ and $b = 3$. The topology of the solution remains unaffected by the choice of model parameters.

General solutions for circular holes in an ionosphere with simple vertical structure are considered next. For $s = 1$ the density disturbance is circularly symmetric with radius r around the (\hat{x}, \hat{y}) origin. The solutions from (12) require $a_0 = 0$ and $a_1 = 1$ with the result

$$\begin{aligned} \hat{r} &= \sqrt{\hat{x}^2 + \hat{y}^2} \\ \hat{\Phi}^{(1)}(\hat{x}, \hat{y}) &= \hat{x} G[\hat{r}] \\ L'_p(\hat{r}, 1) &= - \frac{\{3 + \hat{y} \frac{\partial \log[\Sigma_{p0}(\hat{y})]}{\partial \hat{y}}\} G'(\hat{r}) + \hat{r} G''(\hat{r})}{G(\hat{r}) + \hat{r} G'(\hat{r}) - 1} \end{aligned} \quad (16)$$

To eliminate any dependence on \hat{y} in (16), the background Pederson conductivity takes the functional form

$\Sigma_{p0}(\hat{y}) = C_0 \hat{y}^m$ where m and C_0 are constants. With this substitution, (16) becomes

$$L'_p(\hat{r}, 1) = - \frac{(3 + m)G'(\hat{r}) + \hat{r} G''(\hat{r})}{G(\hat{r}) + \hat{r} G'(\hat{r}) - 1} \quad (17)$$

which is identical to (13) with $a_0 = 0$, $a_1 = 1$ and $m = -1$. The corresponding formula for the spatial variation of Pedersen conductivity is

$$\Sigma_p^{(1)}(\hat{x}, \hat{y}) = \frac{C_0 \hat{y}^m}{G(\hat{r}) + \hat{r} G'(\hat{r}) - 1} \exp \left[-(1+m) \int \frac{G'(\hat{r})}{G(\hat{r}) + \hat{r} G'(\hat{r}) - 1} d\hat{r} \right] \quad (18)$$

Using separation of variables, a wider range of solutions for (7) in cylindrical geometry can be derived but (18) embodies the useful solutions for equatorial bubble modeling.

The one-dimensional ($s=0$) and two-dimensional, circularly-symmetric ($s=1$) expressions are similar. With $a_0 = 0$ and $a_1 = 1$, the rational polynomial function of the form $G(q) = \frac{a}{1+q^b}$ used in (10), and the corresponding potentials from (13) and (14) are

$$\hat{\Phi}^{(0)}(\bar{x}) = \frac{\bar{x} a}{1+|\bar{x}|^b} \quad (19a)$$

$$\text{and } \hat{\Phi}^{(1)}(\bar{x}, \bar{y}) = \frac{\bar{x} a}{1 + (\bar{x}^2 + \bar{y}^2)^{b/2}} \quad (19b)$$

where a and b are constants. Analytic solutions can be obtained from (13) through (16).

Derivatives of the density perturbations become

$$L'(q, 0) = \frac{a b q^{b-1} [1 + b + (1-b)q^b]}{(1+q^b)[a - a(b-1)q^b - (1+q^b)^2]} \quad \text{where } q = |\bar{x}| \quad (20a)$$

$$L'(\bar{r}, 1) = \frac{a b \bar{r}^{b-1} [2 + b + m + (2-b+m)\bar{r}^b]}{(1+\bar{r}^b)[a - a(b-1)\bar{r}^b - (1+\bar{r}^b)^2]} \quad \text{where } \bar{r} = \sqrt{\bar{x}^2 + \bar{y}^2} \quad (20b)$$

The corresponding Pederson conductivity expressions are

$$\Sigma_p^{(0)}(\bar{x}, \bar{y}) = \Sigma_{p0}^{(0)}(\bar{y}) \frac{(1+|\bar{x}|^b)^2}{1 - a - B_1 |\bar{x}|^b + |\bar{x}|^{2b}} \quad (21a)$$

$$\Sigma_p^{(1)}(\bar{x}, \bar{y}) = \exp \left\{ \frac{a(1+m)}{A_1} \left[2 \tan^{-1} \left(\frac{B_1 - 2\bar{r}^b}{A_1} \right) - \text{sign}(a) \pi \right] \right\} \frac{C_0 \bar{y}^m (1+\bar{r}^b)^2}{1 - a - B_1 \bar{r}^b + \bar{r}^{2b}} \quad (21b)$$

where $A_1 = \sqrt{-a[4b + a(b-1)^2]}$ and $B_1 = -a(b-1) - 2$ and $\bar{r} \hat{=} \sqrt{\bar{x}^2 + \bar{y}^2}$. The constants of integration are chosen to yield the background density at large distances where $x \rightarrow \infty$. The physically acceptable solutions have $b > 0$.

The analytic solutions give insight into the relationships between localized density perturbations and the associated electric potentials. Two types of conductivity structures, cavities and enhancements, are described

by (21a and 21b). In the parameter range $\frac{-4b}{(b-1)^2} \hat{=} a_{\text{Min}} > a > 0$, the plasma structure is a cavity centered at

$x = 0$. These limits are found by solving for $A_1 = 0$. As parameter “ a ” approaches the value of “ a_{min} ” the sides of the density cavity becomes steeper. With $a = a_{\text{min}}$, the wall of the cavity is located at radius is

$$\bar{r} = \left(\frac{b+1}{b-1} \right)^{\frac{1}{b}}. \quad \text{For } b > m + 2, \text{ the cavity has a ridge located at } \bar{r} = \left(\frac{b+m+2}{b-m-2} \right)^{\frac{1}{b}}.$$

Quasi-Analytic Models for Density Bubbles and Plasma Clouds in the Equatorial Ionosphere

With $0 > a > 1$, a conductivity enhancement is found at the origin. This enhancement can represent the increased Pedersen conductivity produced by an artificial ion cloud from Barium or similar material released in the sunlit ionosphere. As $a \rightarrow 1$, the sides of the density enhancement become steeper. Solutions exist for all values of $b > 0$ but if $b > 1$, the potential vanishes at large distances. If $a > 1$, then the solutions in (21a and 21b) become complex and are not physically possible. The maximum upward velocity for the potential

$\Phi^{(1)}(x, y)$ in (17b) is $V_{y0} = \frac{1}{B_0} \frac{\partial \Phi(x, y, t)}{\partial x} = \frac{a E_{Tx}}{B_0}$. If $a > 1$, then the conductivity would move with a

velocity larger than the E_{Tx}/B_0 velocity of the driving force, which is not possible. For instance if only a vertical wind U_y is considered in the equation (6) for E_{Tx} , then the upward velocity is $V_{y0} = a U_y$. An unreasonable value of $a > 1$ would permit the conductivity enhancement to rise faster than the neutral wind driver.

The restrictions on the ranges for the potential amplitude “a” indicate that not all electric potentials correspond to a physical density or Pedersen conductivity structure. For a given force on the plasma from external electric fields, neutral winds or gravity, the induced potential is determined by the gradients on the wall of density cavity or enhancement. These gradients are physically limited by infinite steepness and the amplitude of the potential is a maximum at this limit. Thus, for the solution to (4), a given physical density structure will always correspond to a potential function. The magnitude of a potential function can be increased to the point that there is no corresponding plasma density function.

The one dimensional expression (21a) can represent a horizontal density modulation that uniformly changes the background density of a stratified ionosphere. These may be produced by horizontally traveling acoustic-gravity waves can act as seeds for equatorial bubbles. The elongated shapes of these modulations are illustrated by the example in Figure 2. The elongations can be found in nature as the extensions of an ionospheric plume below its top. The horizontal electric field vectors calculated as gradients of the potential yield vertical plasma transport. This transport is normal to the density gradients and, consequently, no net change in the densities is produced. The electric fields near the top of the bubble are the primary drivers for plasma transport. The cylindrical solutions describe the head portion of the bubble. Combining the head and tail portions of the analytic bubbles is discussed in Section 3.

Pedersen Conductivity

Normalized Potential

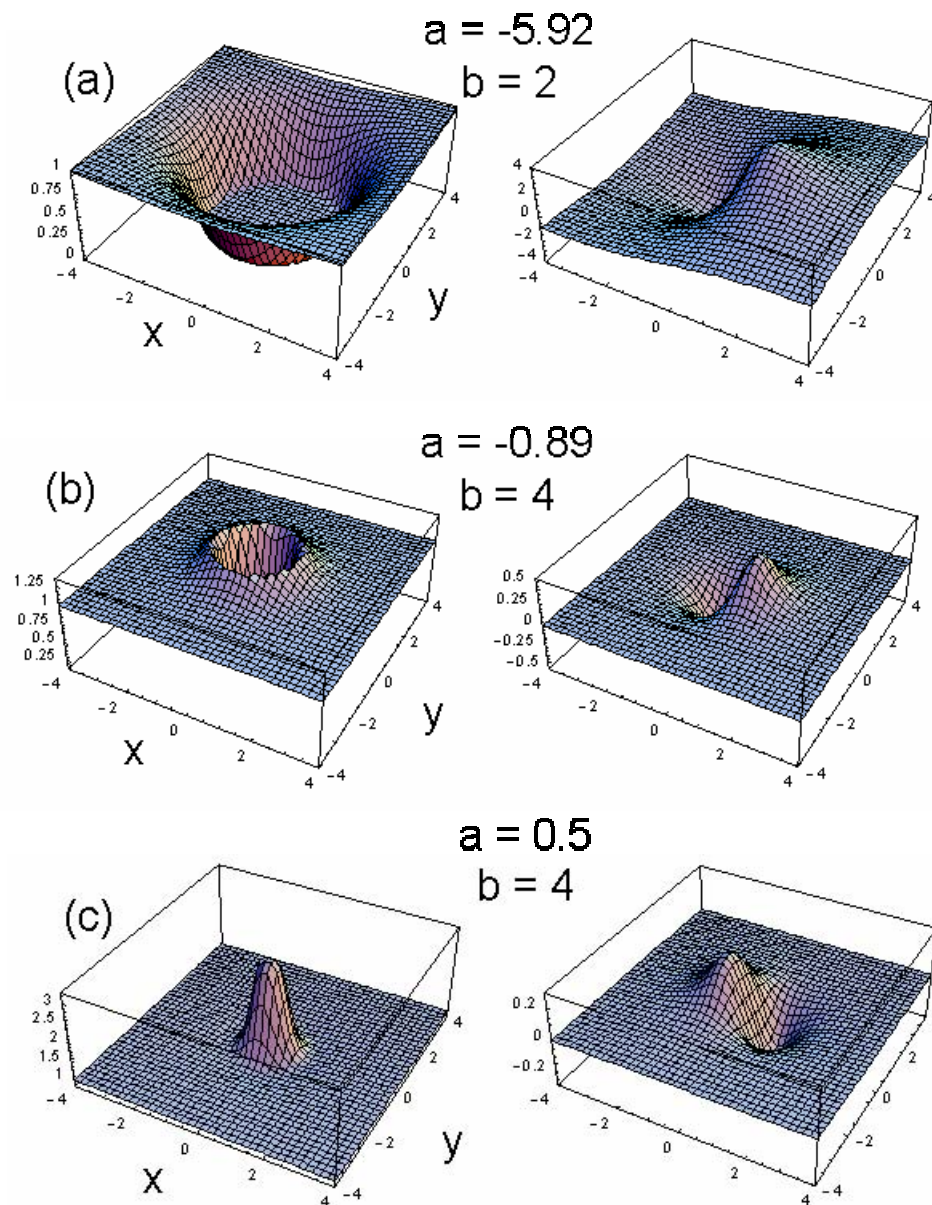


Figure 3. Analytic results for density cavities and enhancements in a uniform background (i.e., $m=0$). The densities and potentials are computed using (a) $b = 2$, $a = 0.99$ $a_{\text{Min}} = -5.92$, and (b) $b = 89$, $a = 0.5$ $a_{\text{Min}} = -0.48$, (c) $b = 4$, $a = 0.5$. The changes in the parameters yield either (a) a cavity with steep sides, (b) a ridge around the cavity or (c) a peaked enhancement.

Quasi-Analytic Models for Density Bubbles and Plasma Clouds in the Equatorial Ionosphere

The two-dimensional solutions to the potential equation are more useful than the one-dimensional solutions. The expression for $\Sigma_p^{(1)}(\hat{x}, \hat{y})$ in (21b) describes a plasma disturbance with two-dimensional structure. The conductivity (or electron density) vanishes in $\Sigma_p^{(1)}(\hat{x}, \hat{y})$ at $y=0$ unless $m=0$. Figure 3 illustrates three examples of the analytic density cavities and the associated electric potential for a uniform background using $m=0$. By changing the parameters in the analytic model, a wide variety of density structures is obtained.

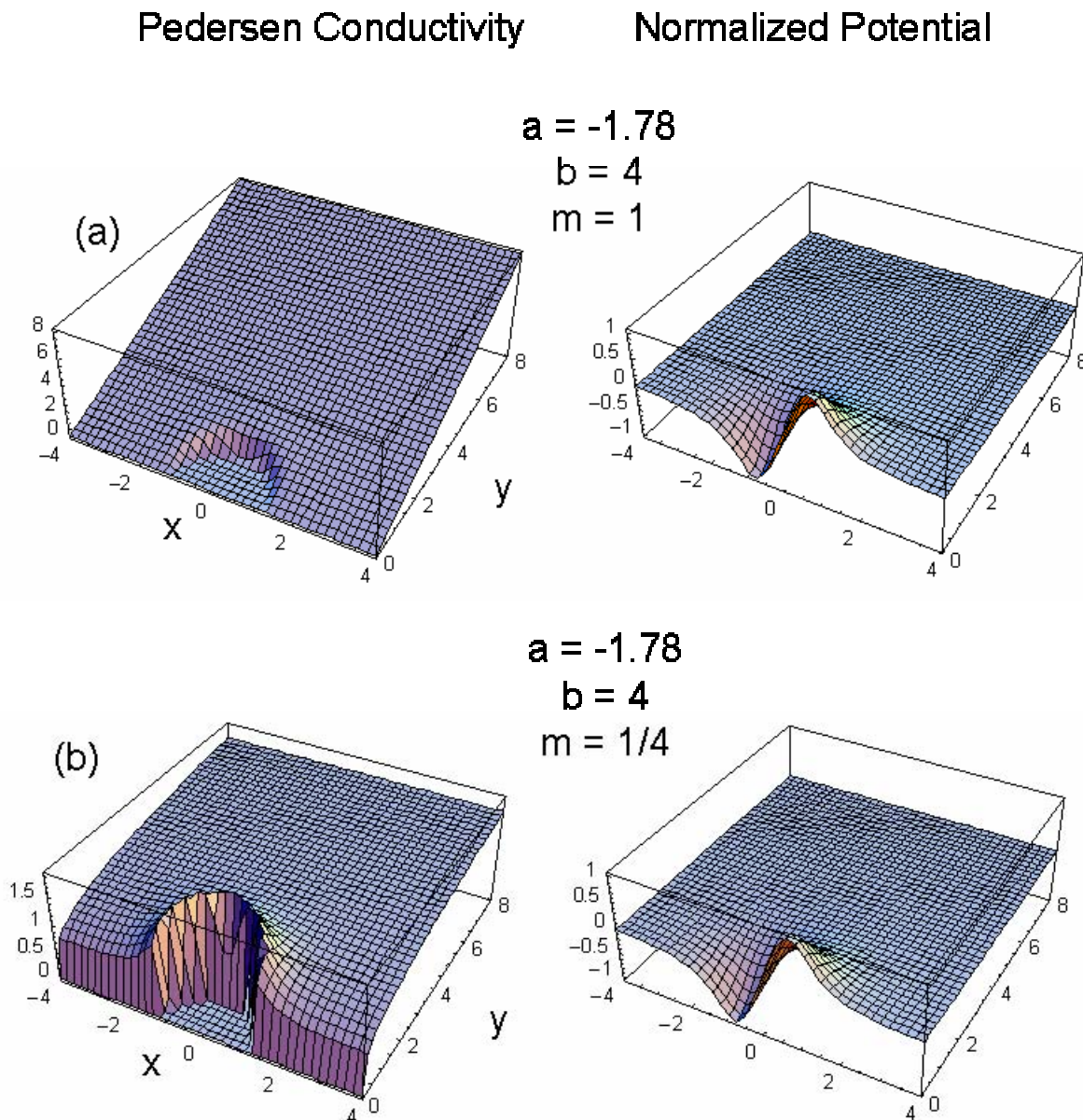


Figure 4. Density cavities imbedded in a linear and inverse-quartic variation for the vertical profile of the plasma conductivity. Both structures yield the same electric potential. The conductivity and the y-directed electric field go to zero at the lower boundary.

The background plasma variation can be approximated using nonzero values of m . The Pedersen conductivity from (21b) vanishes at the $\hat{y} = 0$ boundary if $m > 0$. With $\Sigma_p = 0$ at the lower $\hat{y}=0$ boundary, the potential equation (7) reduces to $\frac{\partial \Sigma_p}{\partial \hat{y}} \frac{\partial \hat{\Phi}}{\partial \hat{y}} = 0$. To satisfy this condition, $\partial \hat{\Phi} / \partial \hat{y} = 0$ because a vertical gradient $\partial \Sigma_p / \partial \hat{y}$ is nonzero-positive at the lower boundary. This condition is automatically built into the analytic expression for the electric potential because of the \hat{y}^2 symmetry of $\hat{\Phi}(\hat{x}, \hat{y}) = \hat{x} G(\sqrt{\hat{x}^2 + \hat{y}^2})$.

Two quantitatively different ionospheres can become polarized with the same potential variation. Figure 4 illustrates two solutions of (21b) with identical parameters for a and b but with (a) $m = 1$ for a linear background profile, and (b) $m = 0.25$ for a forth-root of y profile. As seen by the solutions in (21a and 21b), a family of Pedersen conductivity structures can be associated with a single electric potential (or field) distribution. This non-uniqueness property can be exploited for modeling the evolution of the density structures

3.0 FORMATION OF BUBBLE STRUCTURES FROM ANALYTIC SOLUTIONS FOR TROUGHS AND HOLES

The analytic solutions derived in Section 2.0 are the building blocks for analytic descriptions of equatorial bubble structures. A single plasma bubble or the individual finger of plasma bifurcation can be decomposed into holes and troughs. By adjusting the parameters of the analytic descriptions for the holes and troughs, any finger of a plasma irregularity can be approximated. The procedure for bubble finger formation is based on noting that an analytic potential in (14) with the form $\hat{\Phi}^{(1)}(\hat{x}, \hat{y}) = \hat{x} G_1[\sqrt{\hat{x}^2 + \hat{y}^2}]$ is shown to have a density structure of the form

$$\Sigma_p^{(1)}(\hat{x}, \hat{y}) = \frac{C_0}{G_1(\hat{r}) + \hat{r} G_1'(\hat{r}) - 1} \exp \left[- \int \frac{G_1'(\hat{r})}{G_1(\hat{r}) + \hat{r} G_1'(\hat{r}) - 1} d\hat{r} \right] \quad (22)$$

where $\hat{r} = \sqrt{\hat{x}^2 + \hat{y}^2}$ and $m = 0$.

Analytic bubbles or fingers are formed by using (22) for the top portion or “tip” of the finger above some altitude y_0 and by extending the horizontal, x -axis cross-section downward for the plume portion of the bubble for y less than y_0 . The bubble is then fully described by

$$\Sigma_{\text{Bubble}}(\hat{x}, \hat{y}) = \begin{cases} \Sigma_p^{(1)}(\hat{x}, \hat{y}) & \text{for } \hat{y} > \hat{y}_0 \\ \Sigma_p^{(1)}(\hat{x}, y_0) & \text{for } \hat{y} < \hat{y}_0 \end{cases} \quad (23)$$

Away from the transition altitude y_0 , the corresponding electric potential is given by

$$\hat{\Phi}_{\text{Bubble}}(\hat{x}, \hat{y}) = \begin{cases} \hat{\Phi}^{(1)}(\hat{x}, \hat{y}) = \hat{x} G_1[\sqrt{\hat{x}^2 + \hat{y}^2}] & \text{for } \hat{y} \gg \hat{y}_0 \\ \hat{\Phi}^{(0)}(\hat{x}) = \int_0^{\hat{x}} \left[1 - \Sigma_p^{(1)}(q, \hat{y}_0)^{-1} \right] dq & \text{for } \hat{y} \ll \hat{y}_0 \end{cases} \quad (24)$$

Quasi-Analytic Models for Density Bubbles and Plasma Clouds in the Equatorial Ionosphere

These equations satisfy the normalized potential equation (7) at all locations near $y = y_0$ where the electric potential from one type solution penetrates into the region of the other type solution.

The bubble potential can be thought of as a weighted sum of the analytic solutions for the potentials of the trough and hole. If the end of the trough joins the center of the hole (i.e., $y_0 = 0$) then the potential at that point is the average of the two potentials. This is proven by noting at $y = 0$ that $\frac{\partial \text{Log}[\Sigma_p^{(1)}(\bar{x}, 0)]}{\partial \bar{y}} = 0$ and

therefore $\frac{\partial \text{Log}(\Sigma_{\text{Bubble}})}{\partial \bar{y}} = 0$. Without the y -derivative, the potential equation (7) becomes

$$\frac{\partial^2 \hat{\Phi}_{\text{Bubble}}}{\partial \bar{x}^2} + \frac{\partial \text{Log}(\Sigma_{\text{Bubble}})}{\partial \bar{x}} \frac{\partial \hat{\Phi}_{\text{Bubble}}}{\partial \bar{x}} + \frac{\partial^2 \hat{\Phi}_{\text{Bubble}}}{\partial \bar{y}^2} - \frac{\partial \text{Log}(\Sigma_{\text{Bubble}})}{\partial \bar{x}} = 0 \quad (25)$$

By assuming that $y_0 = 0$, the potential equations for the hole and the trough take similar forms

$$\frac{\partial^2 \hat{\Phi}^{(1)}(\bar{x}, 0)}{\partial \bar{x}^2} + \frac{\partial^2 \hat{\Phi}^{(1)}(\bar{x}, 0)}{\partial \bar{y}^2} + \frac{\partial \text{Log}[\Sigma_p^{(1)}(\bar{x}, 0)]}{\partial \bar{x}} \left[\frac{\partial \hat{\Phi}^{(1)}(\bar{x}, 0)}{\partial \bar{x}} - 1 \right] = 0 \quad (26)$$

and

$$\frac{\partial^2 \hat{\Phi}^{(0)}(\bar{x})}{\partial \bar{x}^2} + \frac{\partial^2 \hat{\Phi}^{(0)}(\bar{x})}{\partial \bar{y}^2} + \frac{\partial \text{Log}[\Sigma_p^{(1)}(\bar{x}, 0)]}{\partial \bar{x}} \left[\frac{\partial \hat{\Phi}^{(0)}(\bar{x})}{\partial \bar{x}} - 1 \right] = 0 \quad (27)$$

Adding (26) and (27) and comparing with (25) immediately yields that the bubble potential as the average of the trough and the hole potentials

$$\hat{\Phi}_{\text{Bubble}}(\bar{x}, 0) = \frac{\hat{\Phi}^{(1)}(\bar{x}, 0) + \hat{\Phi}^{(0)}(\bar{x})}{2} = \frac{\bar{x} G_1[|\bar{x}|] + \int_0^{\bar{x}} [1 - \Sigma_p^{(1)}(q, \bar{y}_0)^{-1}] dq}{2} \quad (28)$$

In general, the bubble potential from a finger structure (23) takes the form

$$\hat{\Phi}_{\text{Bubble}}(\bar{x}, \bar{y}) = \hat{\Phi}^{(1)}(\bar{x}, \bar{y}) g(\bar{x}, \bar{y}) + \hat{\Phi}^{(0)}(\bar{x}) [1 - g(\bar{x}, \bar{y})]$$

where the transition function $g(x, y)$ is bounded by 0 and 1 with the limits

$$g(\bar{x}, \bar{y}) \rightarrow \begin{cases} 0 & \text{for } \bar{y} \ll \bar{y}_0 \\ 1 & \text{for } \bar{y} \gg \bar{y}_0 \end{cases} \quad (29)$$

and for $y_0 = 0$, $g(x, 0) = 1/2$.

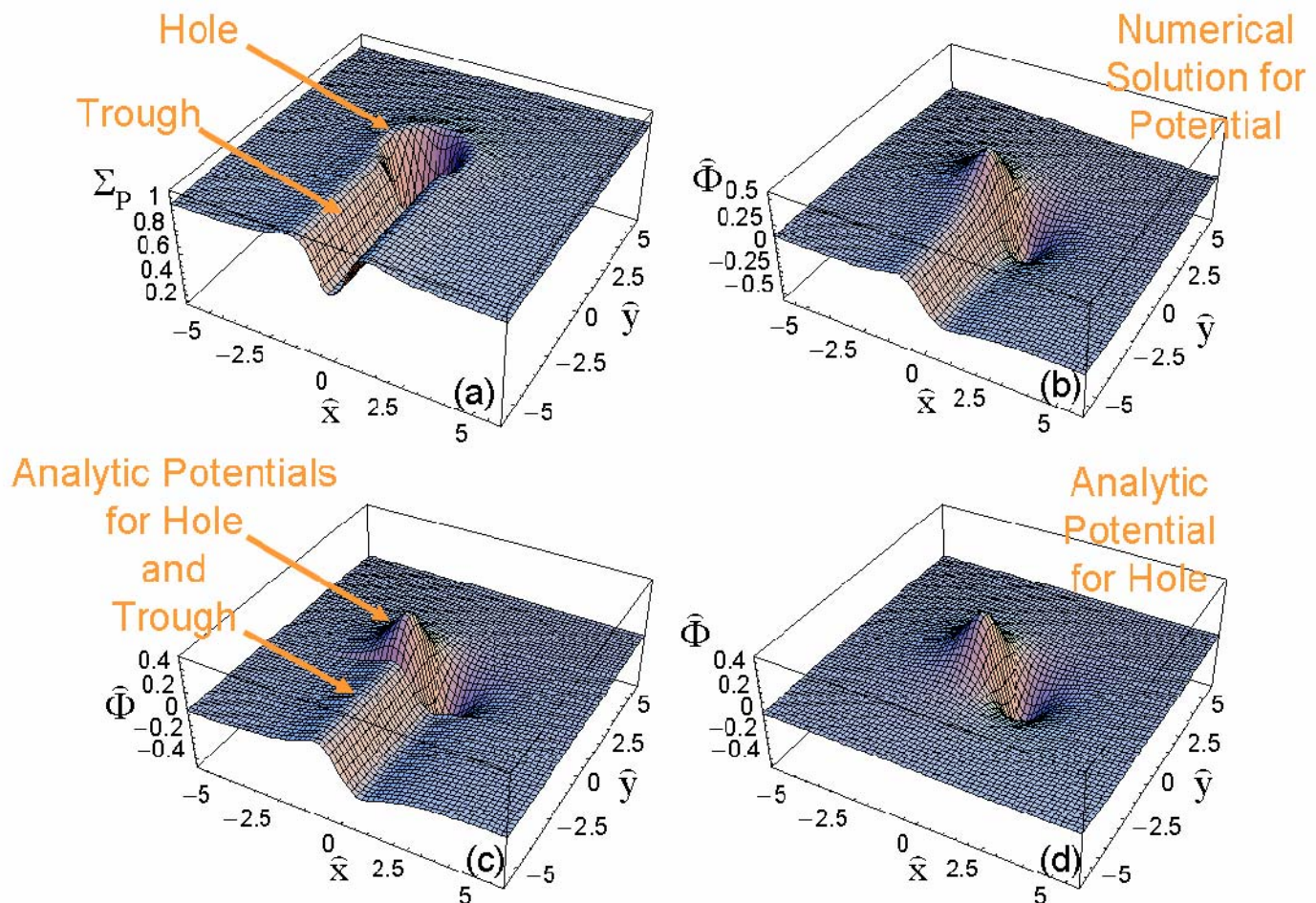


Figure 5. Electric potentials for a plasma bubble (a) formed by attached a plume to a circular density cavity. The numerical solution of the potential equation (b) is approximated by the analytic solutions of the potentials for the plume attached to the potential for the cavity (c). The potential fluctuations at the tip of the bubble closely match the analytic dipole potential (d) associated with the plasma hole.

To illustrate the analytic finger formation, rational polynomial function

$$G_1(q) = \frac{a}{1+q^b} \quad (30)$$

is used to generate density and potential structures. The bubble will be formed in a uniform background plasma by letting $m = 0$. The transition from plume to tip will occur at $y = y_0$ using (21b) to give the analytic result

$$\Sigma_{\text{Bubble}}(\bar{x}, \bar{y}) = \exp \left\{ \frac{a}{A_1} \left[2 \tan^{-1} \left(\frac{B_1 - 2\bar{q}^b}{A_1} \right) - \text{sign}(a) \pi \right] \right\} \frac{(1 + \bar{q}^b)^2}{1 - a - B_1 \bar{q}^b + \bar{q}^{2b}} \quad (31)$$

where $\bar{q} = \sqrt{\bar{x}^2 + \bar{y}^2}$ for $\bar{y} > \bar{y}_0$ and $\bar{q} = \sqrt{\bar{x}^2 + \bar{y}_0^2}$ for $\bar{y} < \bar{y}_0$

Quasi-Analytic Models for Density Bubbles and Plasma Clouds in the Equatorial Ionosphere

The electric potential is found from (24) with $\hat{\Phi}_{\text{Bubble}}(\hat{x}, \hat{y}) = \frac{\hat{x} a}{1 + (\hat{x}^2 + \hat{y}^2)^{b/2}}$ for $\hat{y} > \hat{y}_0$ and the numerical

integral of $\int_0^{\hat{x}} [1 - \Sigma_{\text{Bubble}}(q, \hat{y}_0)^{-1}] dq$ for $\hat{y} < \hat{y}_0$. Figure 5 illustrates the bubble structures for the parameters $a = -0.9$, $b = 3$, and the normalized $y_0 = -1$. The hybrid structure of a trough attached to a hole yields a realistic description for a plasma bubble (Figure 5a). Using a numerical solver for the potential equation (see Appendix A), the electric potential for the analytic bubble structure is computed and is shown in Figure 5b. The hybrid potential (Figure 5c) agrees very well with the computation in all regions except at the interface $y = y_0$ in (23) and (24) where there is a discontinuity in the derivative of the model bubble. For reference, the analytic potential associated with just the tip of the bubble is given in Figure 5d. It turns out that this bubble tip potential is all that is required for computation by the transport equations in the plasma.

The bubble potential drives the plasma transport to change the density of the plasma. The incompressible continuity equation is given by

$$\frac{\partial \Sigma_p}{\partial t} + \mathbf{v} \cdot \nabla_{\perp} \Sigma_p = 0 \quad (32)$$

where the plasma velocity is computed from the electric potential using

$$\mathbf{v} \equiv -\frac{\nabla_{\perp} \Phi \times \mathbf{B}}{B_0}. \quad (33)$$

Normalizations of the potential, derivatives, velocities, and time are given by $\hat{\Phi} = \frac{\Phi}{-E_{Tx} r_0}$, $\hat{\nabla}_{\perp} = r_0 \nabla_{\perp}$, $\hat{\mathbf{v}} \equiv \frac{\mathbf{v} B_0}{-E_{Tx}}$, and $\hat{t} = \frac{-E_{Tx}}{B_0 r_0} t$ with the negative sign for the electric field used

because with downward gravity $E_{Tx} < 0$. With these normalizations, the continuity and plasma drift velocity combined to give the rate of change for the integrated Pederson conductivity

$$\frac{\partial \Sigma_p}{\partial \hat{t}} = -\frac{\hat{\nabla}_{\perp} \hat{\Phi} \times \mathbf{B}}{B_0} \cdot \hat{\nabla}_{\perp} \Sigma_p = \left(\hat{\nabla}_{\perp} \hat{\Phi} \times \hat{\nabla}_{\perp} \Sigma_p \right) \cdot \frac{\mathbf{B}}{B_0} \quad (34)$$

The gradient of the potential (i.e. electric field) must be orthogonal to the gradient in the Pederson conductivity for the densities to change. In the trough portion of the plasma bubble, the density gradients are aligned with the gradients in the potential (Figure 2) and there will be no change in the plasma density in this region where $y < y_0$. Consequently, the primary driver of evolution for the plasma bubbles is the electric potential near the tip of the bubble structures.

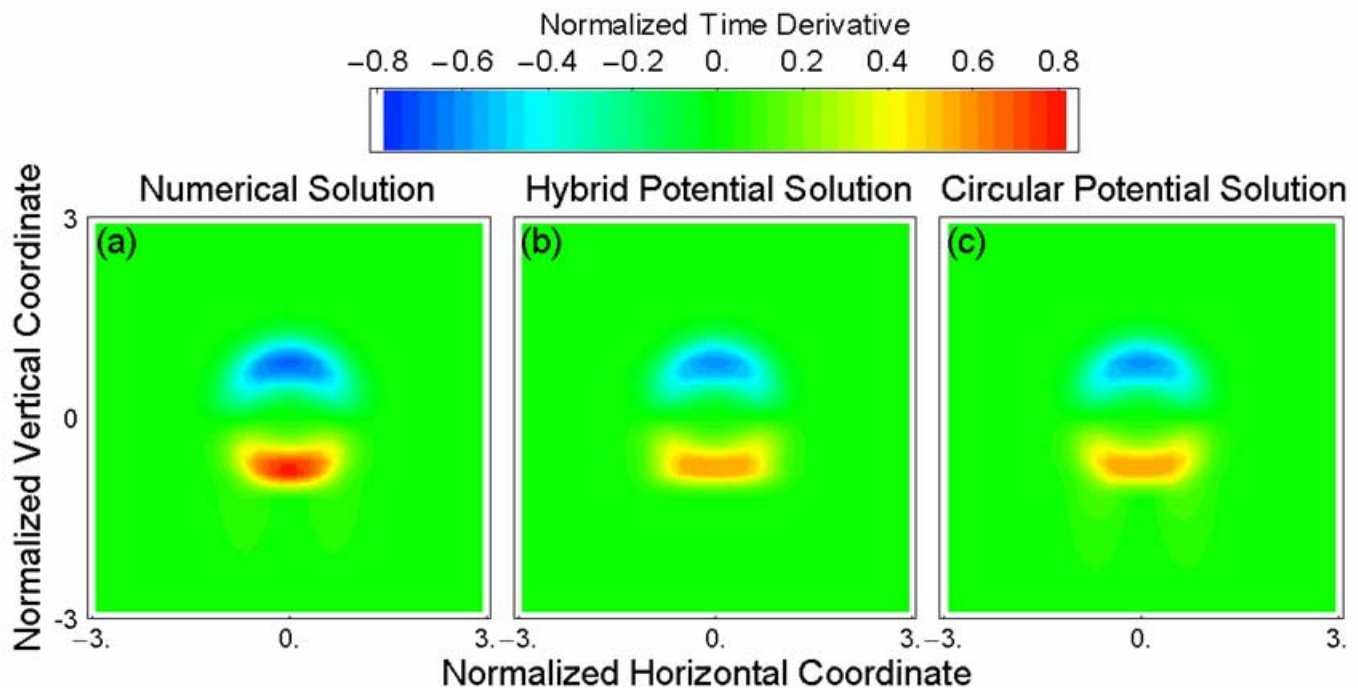


Figure 6. Temporal changes in Pedersen conductivity by incompressible transport from the induced electric fields. The (a) numerical, (b) hybrid, and (c) analytical potentials from Figure 5b, c, and d, respectively, are used to compute the rate of change for the hybrid bubble model shown in Figure 5a. The analytic potential for a plasma hole fit at the tip of the bubble yields a good match to the full numerical solution.

Figure 6 provides a comparison for the conductivity temporal changes of (34) for the model parameters used in Figure 5 for a numerical potential (Appendix A), hybrid analytic potential model (24), and potential for the circular portion of the bubble (19b). All three descriptions of the potential yield a density reduction at the top of the bubble because as the bubble rises, the low density portion of the bubble is transported upward. The density increase at the bottom of the density hole also represents a vertical rise. The transport of the tail portion of the bubble does not provide a change in the density or conductivity. In the case of Figure 6, the electric potential from the circular part of the bubble should be scaled up by 1.2 to provide the correct plasma convection.

From this study, it is concluded that it is sufficient to only consider the electric potential associated with the top portion of the plasma bubble to compute its temporal evolution. The potential of the circular portion of the bubble is most easily found by fitting a plasma density hole such as given by (21b) and then using the fit parameters to describe the potential with the analytic representation of (19b). This procedure provides the basis for the plasma transport algorithm developed in the sections 4 and 5. This discussion justifies the quasi-analytic approach illustrated in Figure 1.

4.0 QUASI-ANALYTIC SOLUTIONS FOR PLASMA TRANSPORT IN A DISTURBED IONOSPHERE

Plasma densities evolve by transport, compression, production and loss. These processes are contained in the continuity equation

Quasi-Analytic Models for Density Bubbles and Plasma Clouds in the Equatorial Ionosphere

$$\frac{\partial n}{\partial t} + \nabla \cdot (n\mathbf{v}) = P - L \quad (35)$$

where n is density, P is production and L is loss. Numerical or analytic solutions to (30) can be based on either the Eulerian or the Lagrangean form of the equations [7]. These forms are equivalent except the Lagrangean form describes where each bit of fluid came from originally. Equation (30) is the Eulerian form of the equation of continuity. The Lagrangean form is derived for the special case of incompressible flow.

The compressibility of a plasma is given by the term $\nabla \cdot \mathbf{v}$. When this term is zero, the plasma is termed incompressible. Using (1) the compressibility of the F-region plasma is found to vanish because

$$\nabla \cdot \mathbf{v} = -\nabla \cdot (\nabla \Phi \times \mathbf{B})/B_0^2 = [-\mathbf{B} \cdot (\nabla \times \nabla \Phi) + \nabla \Phi \cdot (\nabla \times \mathbf{B})]/B_0^2 = 0 \quad (36)$$

where a constant \mathbf{B} is assumed.

Expanding (30) with (31) yields the compressionless form of the continuity equation

$$\frac{\partial n}{\partial t} + \mathbf{v} \cdot \nabla n = \left(\frac{\partial}{\partial t} + \mathbf{v} \cdot \nabla \right) n \equiv \frac{Dn}{Dt} = P - L \quad (37)$$

where Dn/Dt is called the total derivative. The total derivative of the density moves with a small volume element $(\Delta x, \Delta y, \Delta z)$ in the velocity field. During this process a plasma element at (x, y, z) is mapped to another location (x', y', z') in an increment of time Δt . The incremental mapping equation is given by

$$\mathbf{x}' = \mathbf{x} + \mathbf{v}(\mathbf{x})\Delta t \quad (38)$$

where the vectors have components $\mathbf{x} = (x, y, z)$ and $\mathbf{v} = (v_x, v_y, v_z)$. The derivative form of (33) simplifies (32) so that

$$\begin{aligned} \frac{dn(\mathbf{x}, t)}{dt} &= P(\mathbf{x}, t) - L(\mathbf{x}, t) \\ \frac{d\mathbf{x}(t)}{dt} &= \mathbf{v}(\mathbf{x}, t) \end{aligned} \quad (29)$$

If production and loss are neglected, then the electric fields simply move volume elements of plasma in space but the density in each element remains unchanged. Equations (24) are the Lagrangean form of the continuity equation.

An analytic formulation is developed to describe the equatorial bubbles in terms of a mapping function that distorts the ionospheric layer according to the second equation in (24). The mapping function is usually determined with a numerical simulation that calculates the electrostatic \mathbf{E} fields as a function of time and space as an ionospheric bubble or irregularity is formed in the F-layer. Substitution of these fields into (1) yields the transport velocities and the second equation in (24) can be solved to provide the motion of the density coordinates. The transformation of coordinates by this process is given by

$$\mathbf{x}(t) = \mathbf{M}[\mathbf{x}(t_0), t - t_0] \text{ and } \mathbf{x}(t_0) = \mathbf{M}^{-1}[\mathbf{x}(t), t - t_0] \quad (30)$$

and, neglecting production and loss, the electron densities are given by

$$n(\mathbf{x}, t) = n(\mathbf{M}^{-1}[\mathbf{x}, t - t_0], t_0) \quad (31)$$

where the map \mathbf{M}^{-1} transforms the distorted coordinates back to the initial coordinate locations.

Taking the magnetic field to be aligned with the z-direction, the electron density fluctuations are assumed to vary in the 2-dimensional coordinate system (x, y). The coordinate transform map is given as

$$\begin{bmatrix} x(t) \\ y(t) \end{bmatrix} = \begin{bmatrix} M_x(x_0, y_0, t - t_0) \\ M_y(x_0, y_0, t - t_0) \end{bmatrix} \quad (32)$$

where y is altitude, x is zonal distance in a flat earth system and (x₀, y₀) are the initial values for these coordinates at time t₀.

The mapping function $\mathbf{M}(\mathbf{x}, y, t)$ must be one-to-one and invertible and be the identity map where the induced electric potential is zero and the plasma densities are unchanged. Substitution of (1) into (29) yields

$$\frac{d\mathbf{x}(t)}{dt} = -\frac{\nabla\Phi \times \mathbf{B}}{B_0^2} \quad (33)$$

Assuming uniformity along \mathbf{B} in the z-direction, the differential equations governing the coordinated transformations are

$$\frac{\partial x(x_0, y_0, t)}{\partial t} = -\frac{1}{B_0} \frac{\partial \Phi(x, y, t)}{\partial y} \quad \text{and} \quad \frac{\partial y(x_0, y_0, t)}{\partial t} = \frac{1}{B_0} \frac{\partial \Phi(x, y, t)}{\partial x} \quad (34)$$

Differentiating (34) by x₀ and y₀ and using the Poisson's equation

$$\nabla \cdot \mathbf{E} = \nabla \cdot (-\nabla\Phi) = -\left(\frac{\partial^2 \Phi}{\partial x_0^2} + \frac{\partial^2 \Phi}{\partial y_0^2}\right) \quad (35)$$

yields the equations for the velocities

$$\frac{\partial(\partial x / \partial t)}{\partial x_0} = -\frac{\partial(\partial y / \partial t)}{\partial y_0} \quad \text{and} \quad \frac{\partial(\partial x / \partial t)}{\partial y_0} - \frac{\partial(\partial y / \partial t)}{\partial x_0} = -\nabla^2 \Phi \quad (36)$$

The areas between curves of constant x₀ and y₀ are preserved in the transformation and the trajectories of the coordinate transformation follow contours of constant $\Phi(x, y)$. The electric potential is setup by gravity, neutral winds and external electric fields.

Consider the coordinate transformation provided by the analytic potential from (19b) in the previous section

$$\Phi(x, y) = \frac{(x/r_0) a_x r_0 E_{Tx}}{1 + [(x/r_0)^2 + (y/r_0)^2]^{b/2}} = \frac{\hat{x} a_x r_0 E_{Tx}}{1 + \hat{r}^b} \quad (37)$$

Quasi-Analytic Models for Density Bubbles and Plasma Clouds in the Equatorial Ionosphere

where coordinates \hat{x} and \hat{y} are the Cartesian coordinates normalized by a constant scale factor r_0 and constants a_x and b define the shape of the potential.

The plasma transport velocities are

$$\begin{aligned}\frac{\partial \hat{x}}{\partial \hat{t}} &= \frac{b \hat{x} \hat{y} \hat{r}^{b-2}}{(1 + \hat{r}^b)^2} \\ \frac{\partial \hat{y}}{\partial \hat{t}} &= \frac{1 - b \hat{x}^2 \hat{r}^{b-2} + \hat{r}^b}{(1 + \hat{r}^b)^2}\end{aligned}\quad (38)$$

where $\hat{t} = \frac{a_x E_{Tx}}{r_0 B_0} t$ and $\hat{r} = \sqrt{\hat{x}^2 + \hat{y}^2}$.

The maximum upward velocity at the ($\hat{x} = 0, \hat{y} = 0$) origin is given by $V_{y0} = \frac{a_x E_{Tx}}{B_0}$, independent of the potential shape parameter “ b ”. Note that in our example of the downward gravity vector driving the transport, the parameter E_{Tx} from (6) is less than zero and a value of $a_x < 0$ is required to yield an upward velocity. The parameter $a_x < 0$ denotes a density cavity and consequently the center of the cavity is expected to rise against gravity. If the parameter “ a_x ” were greater than zero, the center of the density enhancement would fall as expected under the influence of gravity. For the rest of the discussion, only density cavities will be considered.

The sides of a cavity fall under the influence of gravity. The minimum downward velocity of $V_{y1} = -\frac{a_x E_{Tx}}{B} \frac{(b-1)^2}{4b} = -V_{y0} \frac{(b-1)^2}{4b}$ is found at $\hat{x} = \pm \left(\frac{b+1}{b-1} \right)^{1/b}$ and $\hat{y} = 0$. The Cartesian coordinate system is distorted by the potential inside a conductivity cavity so that the center cells move upward and the side cells move downward.

The analytic model potential with $b = 4$ was previously illustrated in Figure 3b. The corresponding vector field for the plasma velocities (Figure 6a) shows the central uplift of the plasma. As a result of this flow, after normalized time $\hat{t} = 1$ the initially square cells become mapped according to the results shown in Figure 7b. The horizontal (red) and vertical (blue) grid lines become distorted by the vortex flow from the potential. Note that the area in each plasma cell remains constant during this process.

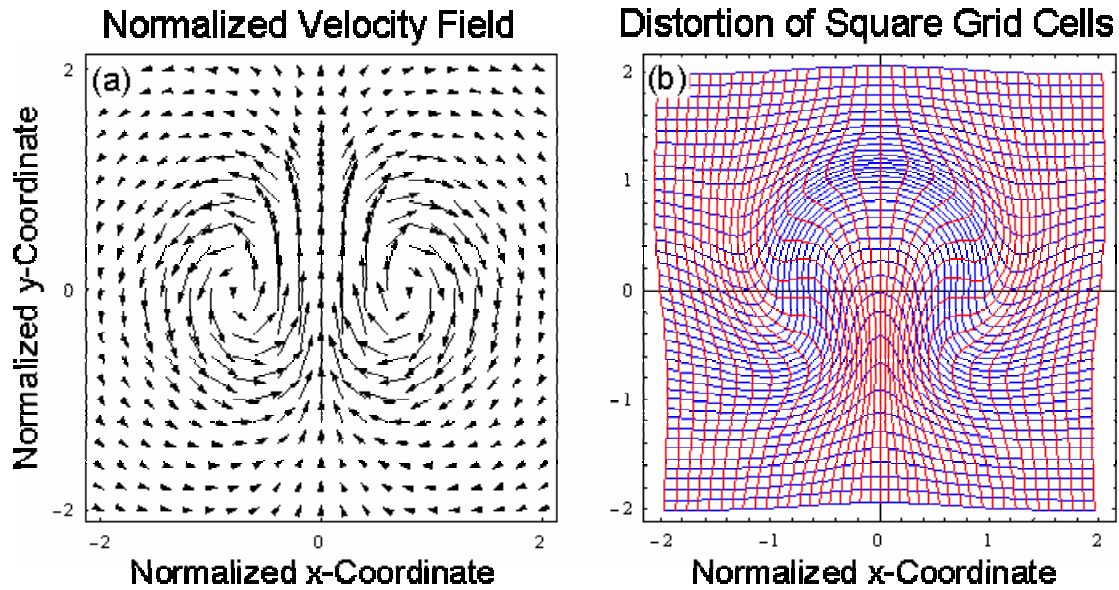


Figure 7. Computed (a) plasma velocities and (b) mapping of Cartesian coordinates by the analytic model for the electric potential shown in Figure 3b. The longest velocity vector has a magnitude

$\frac{a E_{Tx}}{B}$ and the spatial coordinates are normalized by the scale length r_0 . The coordinate map is

illustrated after the flow velocities flow have operated on the plasma for time

$$t = \left(\frac{a E_{Tx}}{B r_0} \right)^{-1} \text{ or when normalized time } \hat{t} = 1.$$

The primary feature of ionospheric bubbles is that they rise leaving an elongated cavity of reduced plasma density often referred to as a “plume”. As the plume rises, it carries the along electric potential. Using the upward velocity for the potential in (32) of $V_{y0} = \frac{a_x E_{Tx}}{B_0}$, the analytic model for the potential becomes

$$\Phi(x, y, t) = \Phi(x, y - V_{y0}t, 0) = \frac{x a_x E_{Tx}}{1 + \left[\left(\frac{x}{r_0} \right)^2 + \left(\frac{y}{r_0} - \frac{V_{y0}t}{r_0} \right)^2 \right]^{b/2}}. \quad (39)$$

With this potential formula, the plasma drift velocities are found from (34) to be

Quasi-Analytic Models for Density Bubbles and Plasma Clouds in the Equatorial Ionosphere

$$\begin{aligned}\frac{\partial \bar{x}}{\partial \bar{t}} &= \bar{x} (\bar{y} - \bar{t}) \frac{b [\bar{x}^2 + (\bar{y} - \bar{t})^2]^{\frac{b-2}{2}}}{\left\{ 1 + [\bar{x}^2 + (\bar{y} - \bar{t})^2]^{\frac{b}{2}} \right\}^2} \\ \frac{\partial \bar{y}}{\partial \bar{t}} &= \frac{1 + [(1-b) \bar{x}^2 + (\bar{y} - \bar{t})^2] [\bar{x}^2 + (\bar{y} - \bar{t})^2]^{\frac{b-2}{2}}}{\left\{ 1 + [\bar{x}^2 + (\bar{y} - \bar{t})^2]^{\frac{b}{2}} \right\}^2}\end{aligned}\quad (40)$$

where the time has been normalized by $\bar{t} = t V_{y0}/r_0$ and $[\bar{x}(0), \bar{y}(0)] = [\bar{x}_0, \bar{y}_0]$ are the initial conditions at time $\bar{t} \equiv \bar{t}_0 = 0$. This equation is the base for the quasi-analytic transport for production of ionospheric bubbles. By using this equation, it is assumed that the electric potential shape is totally specified with fixed parameters E_{Tx} , a , b , and r_0 . The only temporal variation of the potential is that it rises with a constant speed given by

$$V_{y0} = \frac{a_x E_{Tx}}{B_0}.$$

The potential in the trailing portion of the plume is neglected because any vertical flow below the bubble only operates on horizontal gradients and, consequently, there is no net plasma transport within this region.

In the reference frame of the rising potential, $\bar{y}_p \equiv \bar{y} - \bar{t}$ and the differential equations become

$$\begin{aligned}\frac{\partial \bar{x}}{\partial \bar{t}} &= \bar{x} \bar{y}_p \frac{b [\bar{x}^2 + \bar{y}_p^2]^{\frac{b-2}{2}}}{\left\{ 1 + [\bar{x}^2 + \bar{y}_p^2]^{\frac{b}{2}} \right\}^2} \\ \frac{\partial \bar{y}_p}{\partial \bar{t}} &= -1 + \frac{1 + [(1-b) \bar{x}^2 + \bar{y}_p^2] [\bar{x}^2 + \bar{y}_p^2]^{\frac{b-2}{2}}}{\left\{ 1 + [\bar{x}^2 + \bar{y}_p^2]^{\frac{b}{2}} \right\}^2}\end{aligned}\quad (41)$$

The coordinate transformation is found by integrating (41) for (\bar{x}, \bar{y}_p) with an initial value of (\bar{x}_0, \bar{y}_0) and then finding $\bar{y} = \bar{y}_p + \bar{t}$. Further simplification is obtained by transforming to spherical coordinates where $\bar{x} = \bar{r}_p \cos \theta_p$ and $\bar{y}_p = \bar{r}_p \sin \theta_p$. With this substitution, (41) becomes

$$\begin{aligned}\frac{\partial \bar{r}_p}{\partial \bar{t}} &= -\frac{\bar{r}_p^b \sin \theta_p}{1 + \bar{r}_p^b} \\ \frac{\partial \theta_p}{\partial \bar{t}} &= -\frac{\bar{r}_p^{b-1} \cos \theta_p (1 + b + \bar{r}_p^b)}{(1 + \bar{r}_p^b)^2}\end{aligned}\quad (42)$$

where the initial conditions at $\bar{t} = 0$ are $\bar{r}_p(0) = \sqrt{\bar{x}_0^2 + \bar{y}_0^2}$ and $\theta_p(0) = \tan^{-1}(\bar{y}_0/\bar{x}_0)$.

The coordinate transform starts with an electric potential at altitude $\hat{y} \equiv \hat{t}_0 = 0$ and lets this potential distort the coordinates until time \hat{t}_1 when the potential is at altitude $\hat{y} = \hat{t}_1$. The starting and stopping times and altitudes are critical in defining the coordinate distortions. For describing equatorial bubbles, these starting altitude must be transformed to the location where the bubbles starts to form on the bottom side of the ionosphere and the stopping altitude yields with the location of the bubble at time $t_1 = \hat{t}_1 r_0 / V_{y0}$. This renormalization is described later.

The properties of this coordinate transform can be examined at the center where $\hat{x} = 0$ and (40) simplifies to

$$\begin{aligned} \frac{\partial \hat{x}}{\partial \hat{t}} &= 0 \text{ with } \hat{x}(0) = \hat{x}(t) = 0 \\ \frac{\partial \hat{y}}{\partial \hat{t}} &= \frac{1}{1 + [(\hat{y} - \hat{t})^2]^{\frac{b}{2}}} \text{ with } \hat{y}(0) = \hat{y}_0 \end{aligned} \quad (43)$$

The solutions of (43) are found from the nonlinear equation

$$\hat{y} \text{Sign}(\hat{y}_0) + \frac{|\hat{y} - \hat{t}|^{1-b}}{1-b} = |\hat{y}_0| + \frac{|\hat{y}_0|^{1-b}}{1-b} \quad (44)$$

The limiting forms for the asymptotic solutions to (44) are

$$\begin{aligned} \hat{y} &\cong \hat{y}_0 \text{ for } \hat{y}_0 < -1 \\ \left. \begin{aligned} \hat{y} &\cong \hat{y}_0 + \hat{t} \text{ if } \hat{t} < \hat{t}_c \\ \hat{y} &\cong \hat{y}_0 + \hat{t}_c \text{ if } \hat{t} > \hat{t}_c \end{aligned} \right\} \text{ for } -1 < \hat{y}_0 < 0 \text{ and } \hat{t}_c = \frac{(-\hat{y}_0)^{1-b}}{b-1} \\ \hat{y} &\cong \hat{y}_0 \text{ for } 0 \leq \hat{y}_0 \text{ and } \hat{t} < \hat{y}_0 \\ \hat{y} &= \hat{t} \text{ for } \hat{y}_0 = 0 \\ \hat{y} &\cong \hat{t} + \frac{1}{(b-1)^{1/b}} \text{ for } 1 < \hat{y}_0 \text{ and } \hat{t} = \hat{y}_0 \\ \hat{y} &\cong \hat{t} + \left[(b-1)(\hat{t} - \hat{y}_0) + \hat{y}_0^{1-b} \right]^{\frac{1}{1-b}} \text{ for } 0 < \hat{y}_0 \text{ and } \hat{t} < \hat{y}_0 \end{aligned} \quad (45)$$

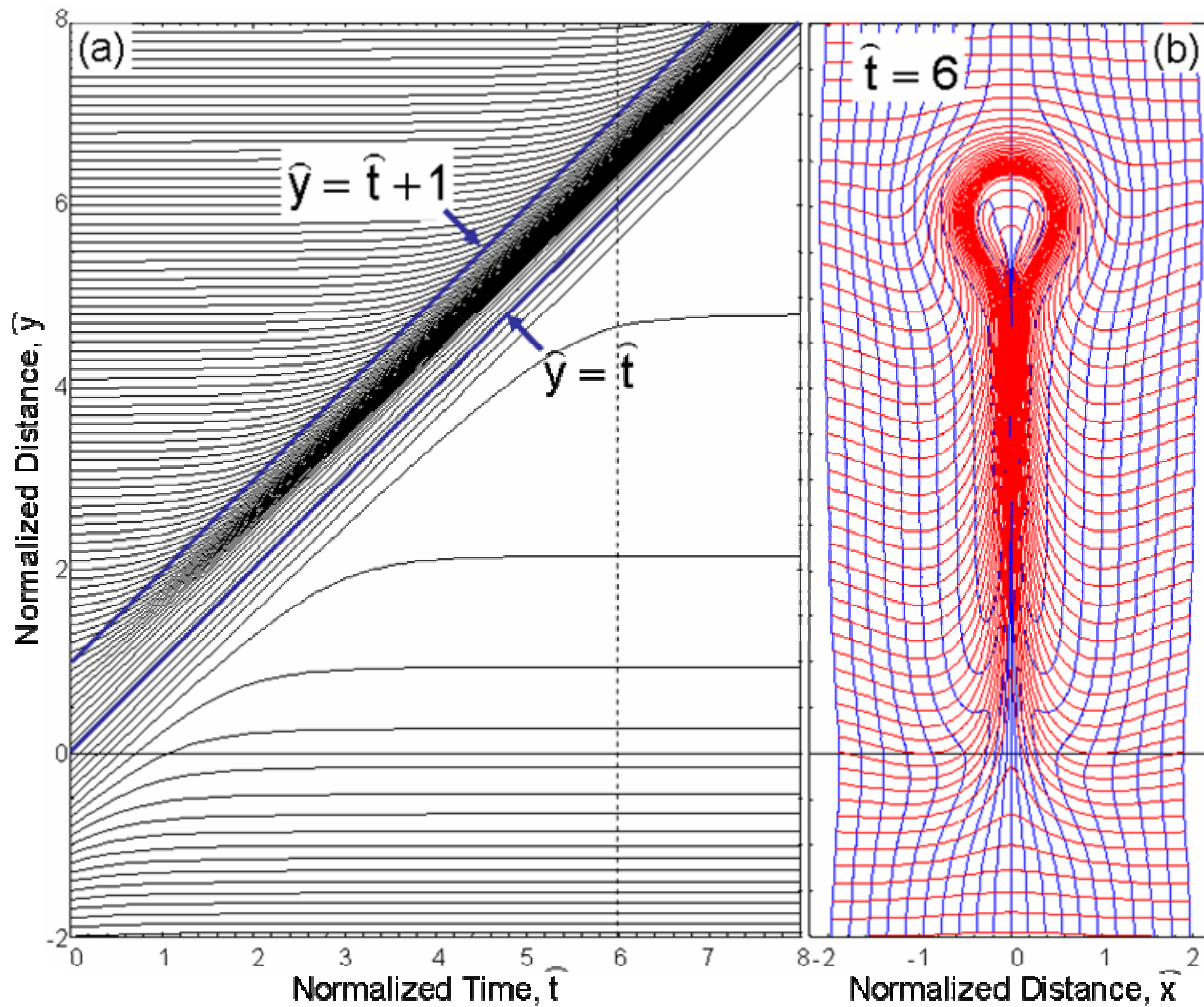


Figure 8. Mapping of the (a) y-axis and (b) a square coordinate grid with a rising potential that starts at the origin. Using equation (34) with $b = 4$, the coordinates above the initial center of the potential are swept into a narrow band that rises with the upward bubble velocity. The snapshot at $\hat{t} = 6$ shows transport of the ionosphere upward at the center and downward at the sides.

This maps of the coordinate distortions are illustrated in Figure 8 using the potential with index $b = 4$. The temporal variations in the normalized altitude are given in Figure 8a. The spatial mapping of the grid at time $\hat{t} = 6$ is shown in Figure 8b. The ionosphere is nearly undisturbed below the starting altitude ($\hat{y} = 0$) of the rising electric potential. The ionosphere is also undisturbed for times ($\hat{t} < \hat{y}_0$) when the potential is below the undisturbed ionosphere. As the potential rises, it sweeps up all the coordinates and carries them in a narrow layer at just above the center of the potential function where $\hat{y} = \hat{t}$. This type of coordinate transformation can be used to simulate the rising equatorial bubble. At time \hat{t}_1 the potential rises to be centered at an altitude $\hat{y}_1 = \hat{t}_1$.

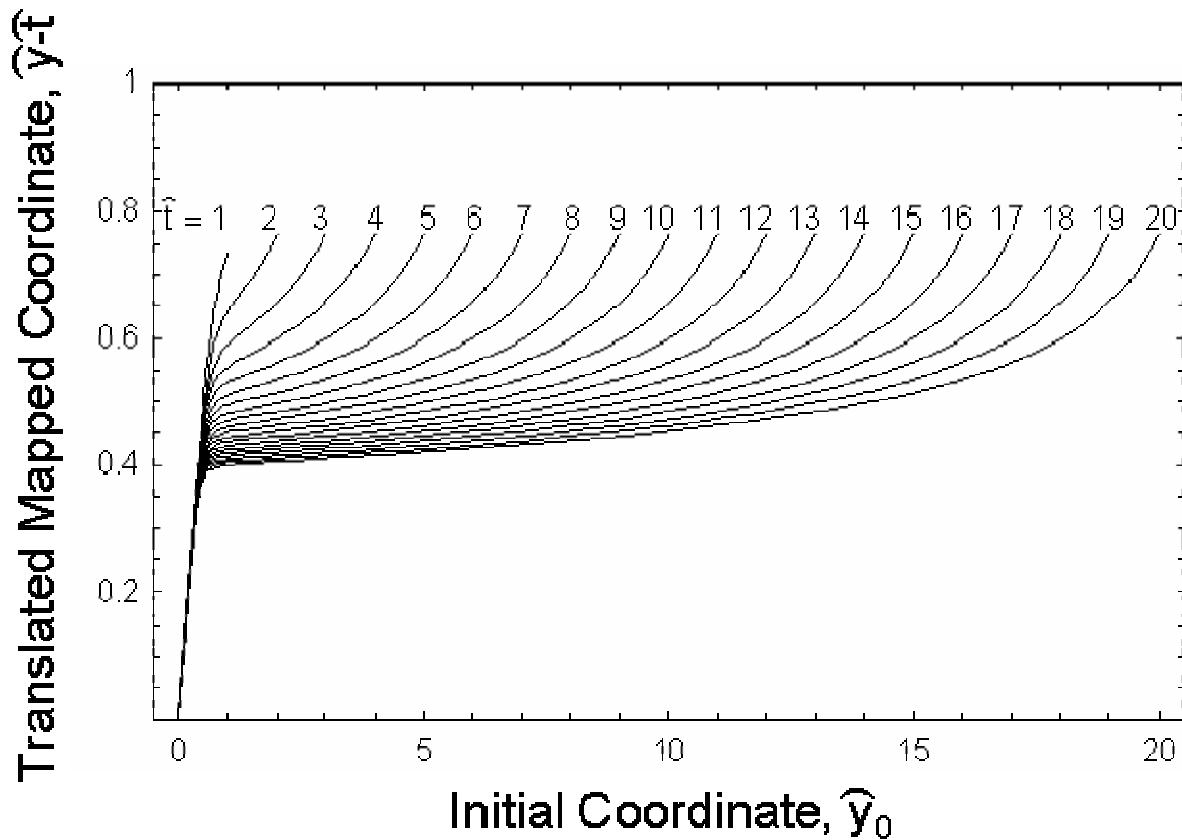


Figure 9. Coordinate compression at the top of the plasma bubble. For the potential parameters $b = 4$, the normalized \hat{y} -coordinates are mapped to a thin shell about 0.4 to 0.45 above the center of the rising potential function located at $\hat{y} = \hat{t}$.

The horizontal coordinates near the center of the rising potential map to a thin shell centered at the altitude $\hat{y} = \hat{t}$. An approximation to this map is given by the last equation in (45). The evolution of this coordinate “compression” is illustrated in Figure 9 for normalized times between $\hat{t} = 1$ and 20 using the parameter $b=4$ for the electric potential. The offset $(\hat{y} - \hat{t})$ from the center of the rising bubble increases monotonically but slowly as the initial coordinate covers a much larger range.

The normalized density gradient at the edge of the bubble is $\frac{\partial n_e}{\partial \hat{y}} = \frac{\partial n_e}{\partial \hat{y}_0} \frac{\partial \hat{y}_0}{\partial \hat{y}}$ so $\frac{\partial \hat{y}_0}{\partial \hat{y}}$ is the coordinate compression factor. Analytically, this factor is given by

$$\frac{\partial \hat{y}_0}{\partial \hat{y}} = \left(\frac{\hat{y}_0}{\hat{y}} \right)^b \frac{1 + \hat{y}^b}{1 + \hat{y}_0^b} \quad (46)$$

Quasi-Analytic Models for Density Bubbles and Plasma Clouds in the Equatorial Ionosphere

This factor is plotted in Figure 10 with $b = 4$ for a wide range of times and initial coordinate altitudes. The compression factor increase with time easily attaining values greater than 10 or 100. With this compression, a bottomside ionospheric gradient becomes greatly amplified as the bubble rises.

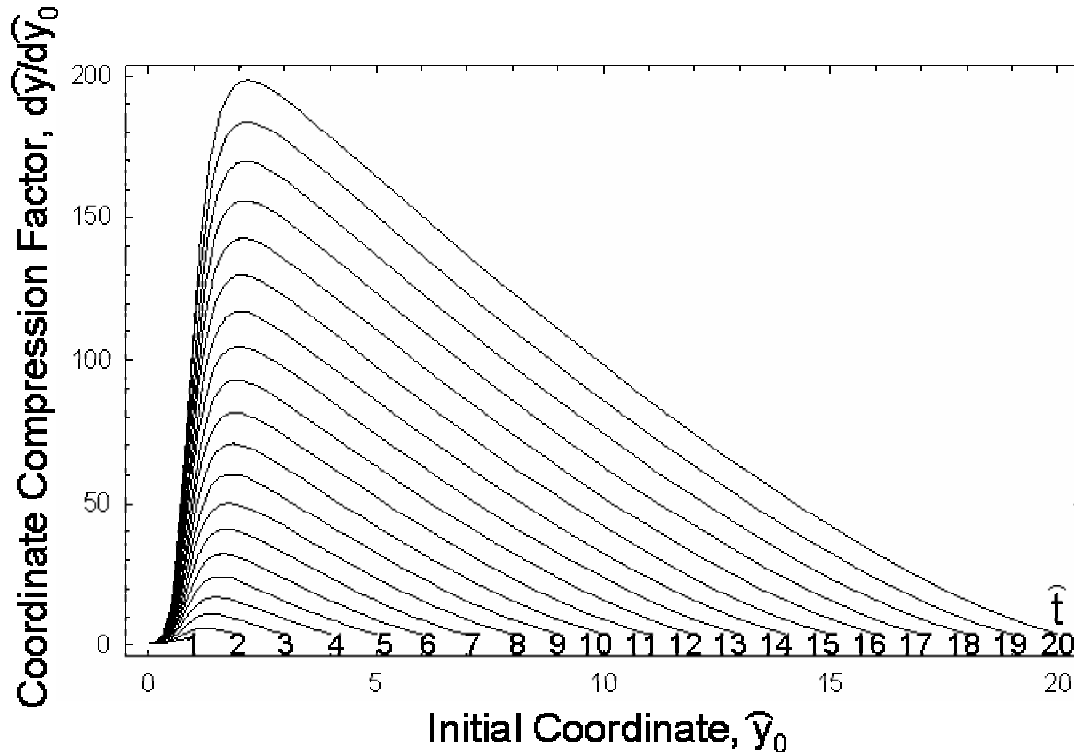


Figure 10. Density gradient enhancement factor for the coordinate compression at the top of the rising bubble with index $b = 4$. The compression becomes enhanced with increases in the normalized time \hat{t} . Outside the effect of the potential this factor is unity. This processes yields the steepened gradients at the sides of the ionospheric bubble.

To obtain the electron density or Pedersen conductivity at time (\hat{t}) , cell coordinates must be obtained for the original cell that was transported to the current position. The model ionospheric bubble is therefore formed by operating on a horizontally stratified layer with the *inverse* of the coordinate transformation defined by (40). This inverse may be obtained with by (1) interpolation of the solution to (40) or (2) by reversing time for the solution of (35). Figure 8 shows the location of the coordinates at the current time for each normalized

starting position $(\hat{x}_0, \hat{y}_0) \equiv \left(\frac{x_0}{r_0}, \frac{y_0}{r_0} \right)$. The interpolation process is hampered by the distortion of the

coordinate density cells. In the mapping shown by Figure 8b, the square cell with corners at $(\hat{x}_0, \hat{y}_0) = (0, 2), (0.1, 2), (0.1, 2.1),$ and $(0, 2.1)$ are mapped to the elongated region with corners $(0, 6.421), (0.1075, 4.374), (0.1112, 4.443), (0, 6.424)$ at $\hat{t} = 6$. With linear interpolation, the point $(\hat{x}, \hat{y}) = (0.055, 5.4)$ inside the elongated region is determined to map to the initial position $(\hat{x}_0, \hat{y}_0) = \{0.0505, 2.0364\}$. This is in error; the correct location for this position is $(\hat{x}_0, \hat{y}_0) = (0.3329, -0.1784)$. Beside being prone to error, this technique

requires interpolation on a non-uniform mesh or numerical solution for the inverse of interpolation on an a uniformly spaced mesh of the coordinate locations at time $\hat{t} = 0$. For good accuracy and ease of computation, interpolation or numerical inverse solutions should be avoided.

Since the electric potential does not evolve with time, the inverse coordinate mapping is easily achieved with time reversal. Consider a cell with location (x_1, y_1) at time $t = t_1$. Running time backwards to time $t = 0$ yields its starting point (x_0, y_0) . If the parameters v_{y0} and b are constant, the time reversal solution is most easily obtained by replacing \hat{t} with $-\hat{t}$ in (35) through (37). This process yields the map represented by (31).

The equations for the inverse coordinate map are

$$\begin{aligned} \frac{\partial \hat{x}_0}{\partial \hat{t}} &= -\hat{x}_0 (\hat{y}_0 + \hat{t}) \frac{b \left[\hat{x}_0^2 + (\hat{y}_0 + \hat{t})^2 \right]^{\frac{b-2}{2}}}{\left\{ 1 + \left[\hat{x}_0^2 + (\hat{y}_0 + \hat{t})^2 \right]^{\frac{b}{2}} \right\}^2} \\ \frac{\partial \hat{y}_0}{\partial \hat{t}} &= -\frac{1 + [(1-b) \hat{x}_0^2 + (\hat{y}_0 + \hat{t})^2] \left[\hat{x}_0^2 + (\hat{y}_0 + \hat{t})^2 \right]^{\frac{b-2}{2}}}{\left\{ 1 + \left[\hat{x}_0^2 + (\hat{y}_0 + \hat{t})^2 \right]^{\frac{b}{2}} \right\}^2} \end{aligned} \quad (47)$$

The center of the potential function starts at altitude $\hat{y}_0 = \hat{t}_1$ and then (47) solved as the center of the potential falls to an altitude $\hat{y}_0 = 0$. For this reason, the inverse coordinate map equations are integrated from $\hat{t} = -\hat{t}_1$ to $\hat{t} = 0$. The initial conditions for (47) are

$$\hat{x}_0(-t_1) = \hat{x}_1 \text{ and } \hat{y}_0(-t_1) = \hat{y}_1 \quad (48)$$

The inverse coordinate map is illustrated in Figure 11 for the initial grid and the distorted inverse grid at several times. This map is used to determine the origin of a coordinate cell and the initial electron density or Pedersen conductivity in that cell. As an example of using this inverse map, the mapping of specific point (0.055, 5.4) is directly obtained with (47) to yield the correct initial location (0.3329, -0.1784).

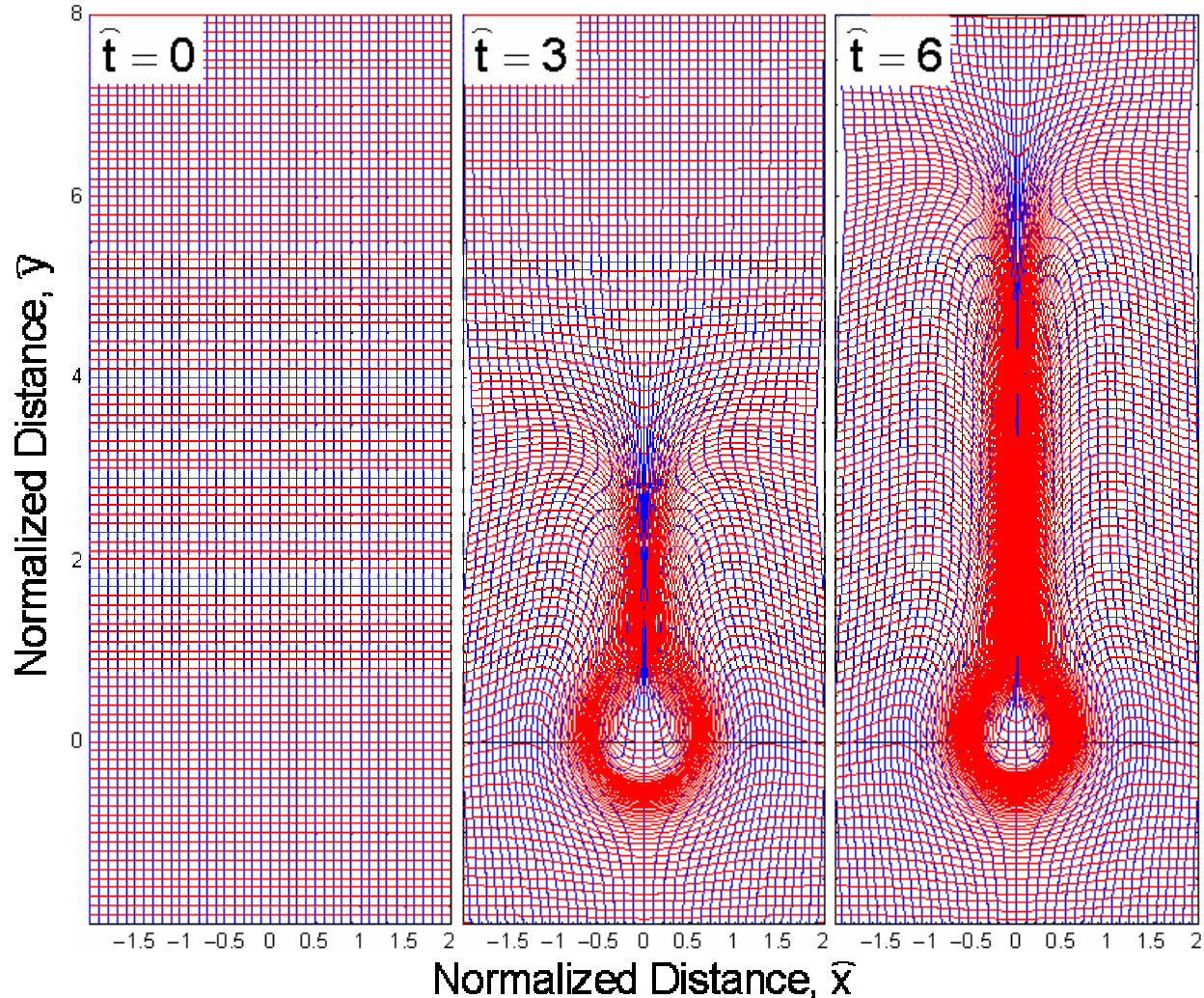


Figure 11. Inverse coordinate map showing source regions for density gradients.

No analytic solution to (47) could be found but the numerical solution to the coupled ordinary differential equations is fast and efficient using standard explicit methods. The Lagrangean inverse-map is consequently called quasi-analytic because no finite-difference approximations are applied to the spatial (x , y) coordinates but discrete steps in the time dependent solutions of (47) is required. Applying the inverse map to any analytical model of a uniform ionosphere can efficiently provide the density at any point in space and time that can be obtained without the use of interpolation or the numerical solution of two-dimensional partial differential equations.

As an example, the inverse coordinate map is applied to an F-layer described by the following formula for a modified Chapman layer.

$$N_e(y) = N_{e0} \text{Exp}[1 - z - \text{Exp}(z)]$$

$$z = \frac{y - H_p}{H_0} \quad (49)$$

$$H_0 = H_{01} + [0.5 + \text{Tan}^{-1}(\frac{y - H_p}{H_1}) / \pi] H_{02}$$

The parameters N_{e0} , H_p , H_0 , H_{01} , H_{02} and H_1 control the shape of the layer. The analytic simulation uses peak density $N_{e0} = 10^6 \text{ cm}^{-3}$, peak altitude $H_p = 400 \text{ km}$, bottom-side scale height $H_{01} = 20 \text{ km}$, top-side scale height $H_{02} = 50 \text{ km}$, and transition scale $H_1 = 10 \text{ km}$. This simple layer model has a steep bottomsides representative of the equatorial ionosphere. The conversion from normalized coordinates is $y = \hat{y} r_0 + y_{c0}$ where y_{c0} is the starting altitude of the electric potential at time $t = 0$.

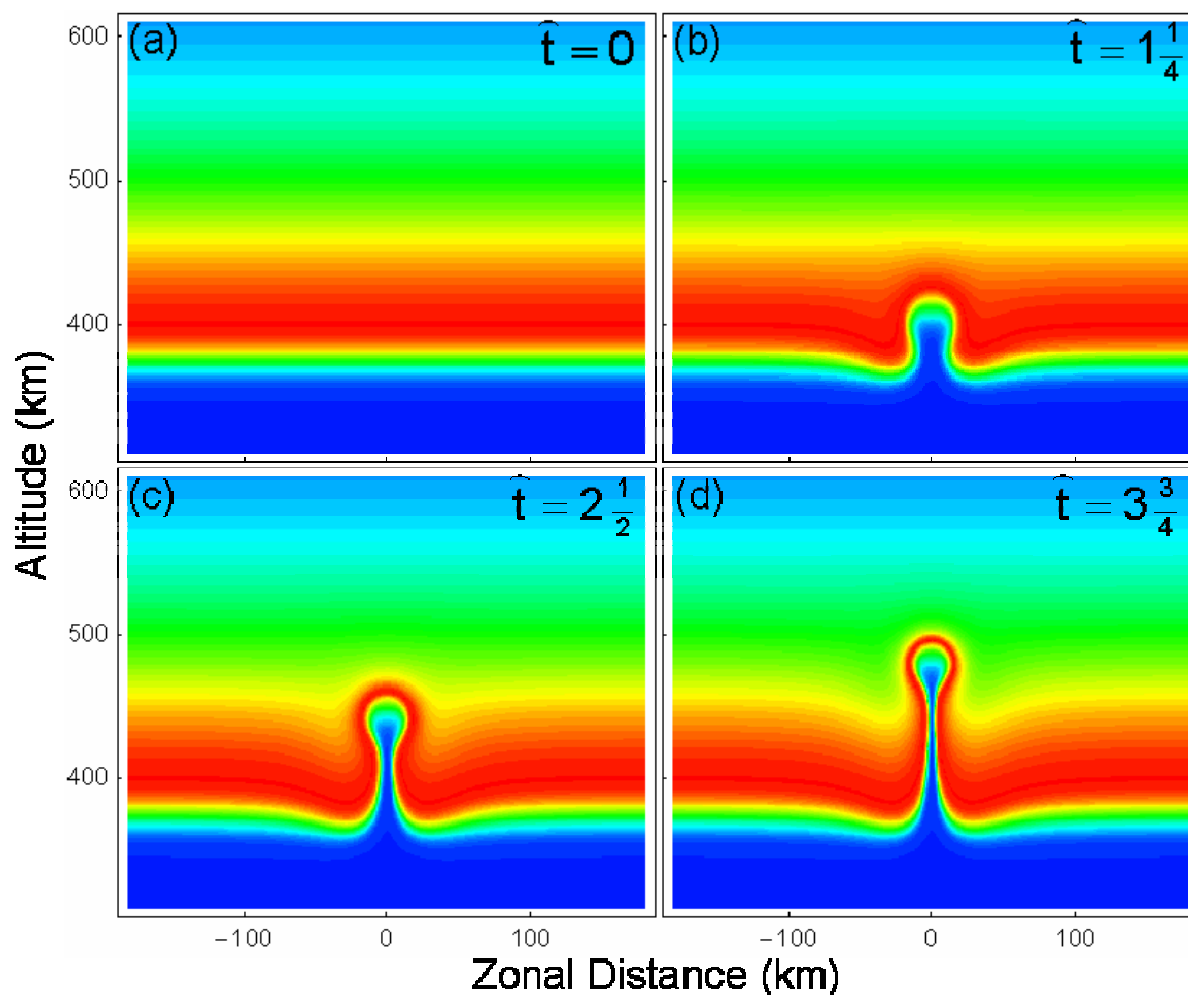


Figure 12. Simulation of a bubble formed in the ionosphere using a simple formulation for the electric potential. The parameters for the model are $b=4$, and $r_0 = 30 \text{ km}$.

Quasi-Analytic Models for Density Bubbles and Plasma Clouds in the Equatorial Ionosphere

Applying the inverse coordinate transformation (47) to the ionospheric profile yields the bubble evolution illustrated in Figure 12. The coordinate distances are determined using a scaling factor $r_0 = 30$ km and the potential function rises through the layer starting at $y_{c0} = 370$ km altitude. The potential function index is arbitrarily set to $b = 4$ for this example. The normalized time coordinate $\hat{t} = t V_{y0}/r_0 = t a_x E_{Tx}/(B r_0)$ is used because the parameter “ a_x ” has yet to be specified. The allowable values for a were previously given after (19) as $\frac{-4b}{(b-1)^2} < a < 0$. With a larger value of parameter “ $a_x E_{Tx}$ ”, the vertical velocity of the bubble increases and the absolute time (t) in the simulation is reduced for a fixed normalized time. Figure 12 illustrates that the analytic model using the rising potential yields a quasi-analytic solution that resembles numerical solutions requiring much more computation time.

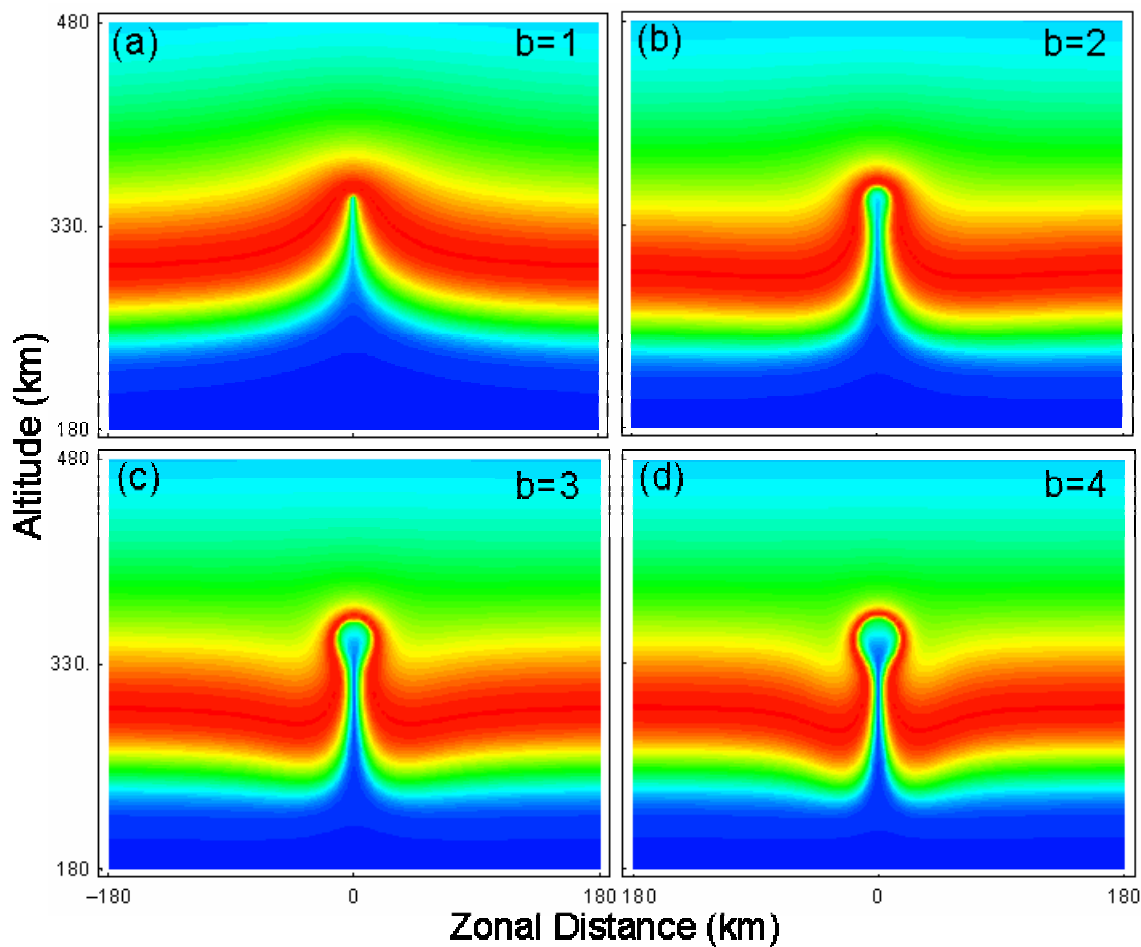


Figure 13. Effect of electric potential index b on the model ionospheric bubble. The normalized time for each solution is $\hat{t} = 3.75$.

Whereas the parameter “ a_x ” controls the bubble rise rate, the “ b ” determines the size of the bubble. The parameter “ b ” may have any value greater than unity. Larger values of b yield electric potentials with larger gradients at the edges. Increasing b increases the region affected by the electric potential. Figure 13

illustrates the ionospheric bubble for several values of this index. Values of the potential index in the range $2 < b < 4$ seem to yield reasonable descriptions of the rising ionospheric bubble.

5.0 BUBBLE TILTS AND AMBIENT SHEAR FLOW

Both observations and numerical computations [8] have demonstrated that neutral winds can tilt the ionospheric plumes off vertical. When acted on by a zonal neutral wind U_x , a vertical electric field E_y is produced by interactions with the background electron density (or Pedersen conductivity). Also, a perturbation electric field E_{Ty} is produced by polarization of the plasma density bubble by the neutral wind. These two processes work simultaneously to affect the tilt the bubbles. First, the background neutral wind induces large scale plasma motions in the zonal, eastward direction. The shear in this large-scale plasma drift will cause the regions of lower background Pedersen conductivity to lag behind the regions of maximum Pedersen conductivity. Second, polarization of the ionospheric bubbles by the neutral wind, which moves faster than the bulk motion of the plasma, will produce horizontal motion that will cause the density depletions to move in the opposite direction of the neutral wind relative to the bulk plasma drift. This is a well known property of plasma holes as they respond to neutral winds [2]. Both of these processes are easily incorporated in the quasi-analytic bubble model.

Vertical gradients in the background density yield vertical gradients in the induced electric field and vertical shears in the horizontal plasma drifts produced by these fields. This process is captured in (2) assuming that the vertical currents vanish with the result

$$J_y = [E_y - U_x B_0] \sigma_p = 0 \quad (50)$$

The field line is divided into the F-region where the wind is uniform and the E-region where the neutral wind will assume to vanish [8]. Calling the integrated Pedersen conductivity in these two regions Σ_F and Σ_E respectively, the vertical electric field profile is given by

$$E_y(y) = \frac{U_x B_0 \Sigma_F(y)}{\Sigma_E + \Sigma_F(y)} \equiv -\frac{\partial \Phi_0}{\partial y} \quad (51)$$

where Φ_0 is the polarization potential of the background plasma.

The resulting plasma velocity is given by (24) with the result

$$\frac{\partial x}{\partial t} = \frac{E_y}{B_0} = U_x \frac{\Sigma_F(y)}{\Sigma_E + \Sigma_F(y)} = U_x \frac{1}{\hat{f}(y/r_0) + 1} \equiv V_{xs} \quad (52)$$

$$\text{where } \hat{f}(y/r_0) = \hat{f}(\hat{y}) = \frac{\Sigma_E}{\Sigma_F(y/r_0)}. \quad (53)$$

This is the horizontal velocity of the plasma in which the bubble is imbedded. Usually the wind shear variation is small compared to the average bulk motion.

Quasi-Analytic Models for Density Bubbles and Plasma Clouds in the Equatorial Ionosphere

In normalized coordinates, this wind shear equation for the background horizontal motion becomes

$$\frac{\partial \bar{x}}{\partial \bar{t}} = \frac{V_{xs}}{V_{y0}} = \frac{U_x}{V_{y0}} \frac{\Sigma_F(y/r_0)}{\Sigma_E + \Sigma_F(y/r_0)} = \frac{U_x}{V_{y0}} \frac{1}{1 + \bar{f}(\bar{y})} \equiv \hat{V}_{xs}(\bar{y}) \quad (54)$$

Integration of (49) yields the simple coordinate map from this large scale plasma motion

$$\bar{x}(\bar{t}) = \int \hat{V}_{xs}(\bar{y}) d\bar{t} = \bar{x}_0 + \bar{t} \hat{V}_{xs}(\bar{y}) \quad (55)$$

where x_0 is the initial coordinate at time $\bar{t} = 0$.

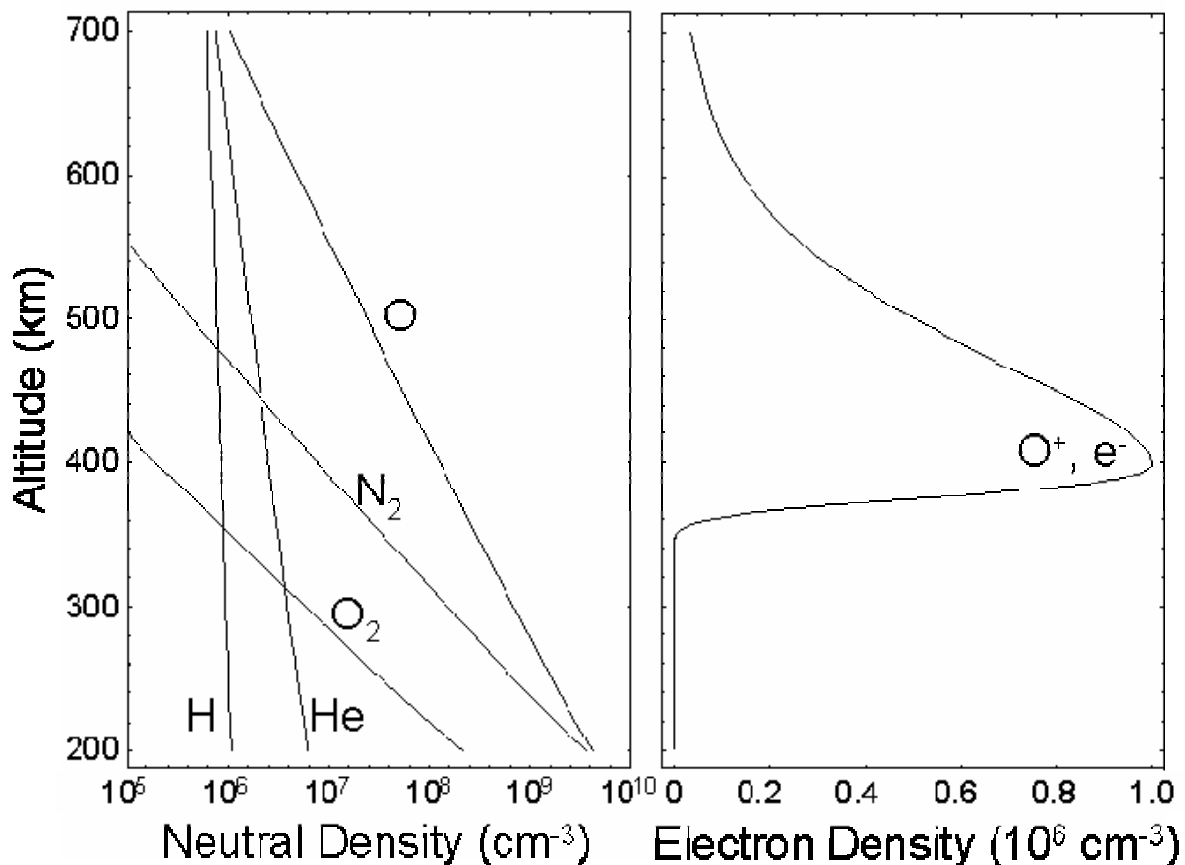


Figure 14. Profiles from neutral atmosphere and electron density models used for the sample computations of electric polarization that tilts the equatorial bubbles.

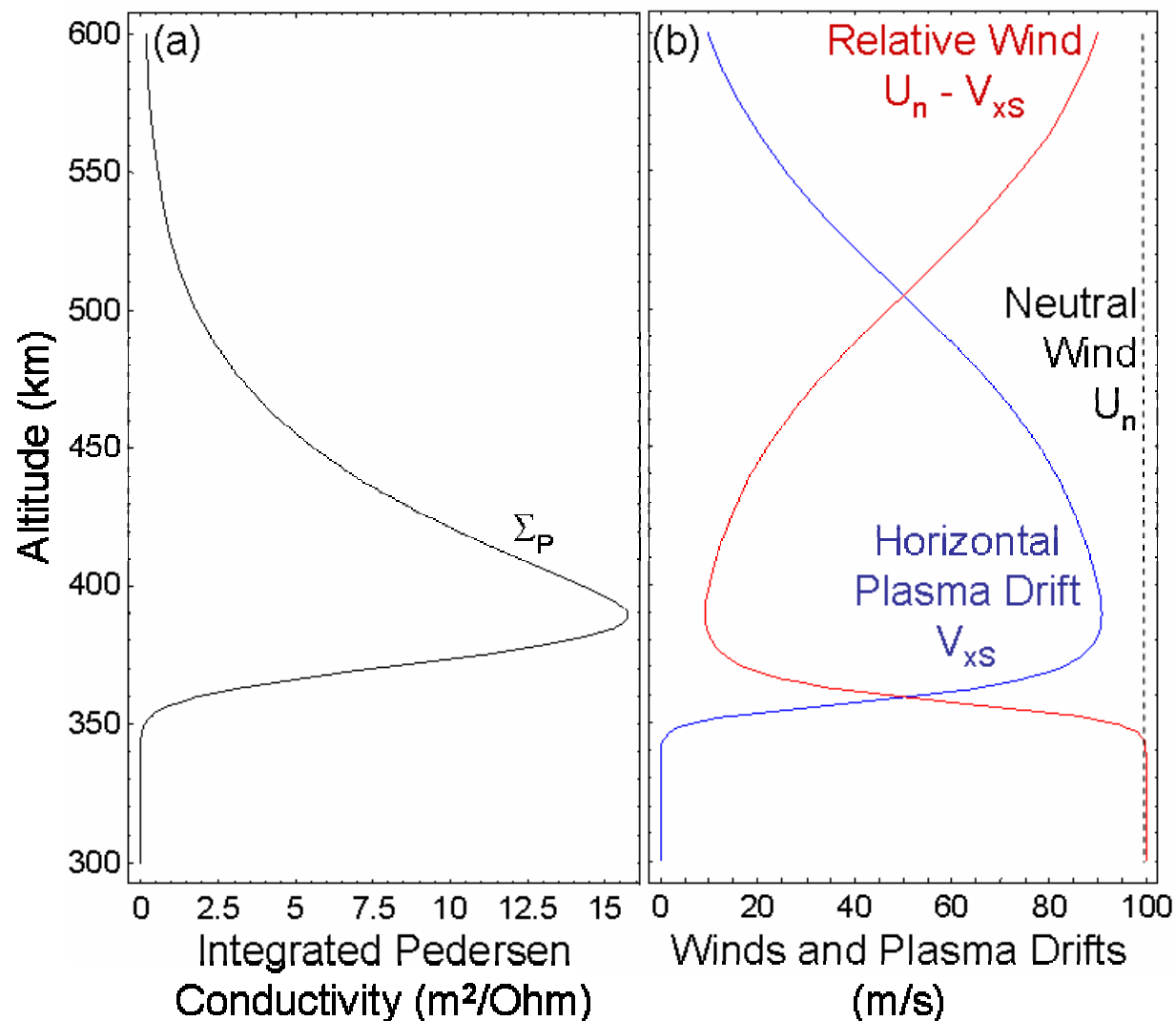


Figure 15. Model profiles of field-line integrated Pedersen conductivity, uniform neutral wind, large-scale horizontal plasma drifts, and horizontal wind relative to the drifting plasma.

If the E-region Pedersen conductivity is zero, then the plasma will move horizontally with the neutral wind speed U_x . A finite Σ_E coupled with vertical shears in the F-region Pedersen conductivity gives a shear structure to the horizontal plasma motion. The tilts of the equatorial plume structures will be computed using the Lagrangean approach to the plasma transport with both imbedded potential given by (39) and the large scale distortions described by (55).

As an example of this wind induced shear in the horizontal plasma drift, a uniform neutral with $U_x = 100$ m/s was used to polarized the plasma layer given by (49) with a peak density of 10^6 cm^{-3} . The model neutral atmosphere and electron density profiles illustrated in Figure 14 are used to derive the equatorial profile of the field-line integrated Pedersen conductivity shown in Figure 15. A dipole magnetic field model of the form

Quasi-Analytic Models for Density Bubbles and Plasma Clouds in the Equatorial Ionosphere

$$B_r = \frac{2 H_0 \cos\theta}{r^3} \text{ and } B_\theta = \frac{H_0 \sin\theta}{r^3} \quad (56)$$

is used for the magnetic field lines where $H_0 = -0.311 \cdot 10^{-5}$ Tesla. Figure 16 illustrates the distortion of a square mesh using the coordinate transform defined by (52). Application of this transform after the transform illustrated in Figure 8 will tilt the bubble to the left (west) side of the simulation. The simulation for Figure 16 used a fixed E-region conductivity Σ_E that was one-tenth the maximum value of the F-layer Pedersen conductivity Σ_F .

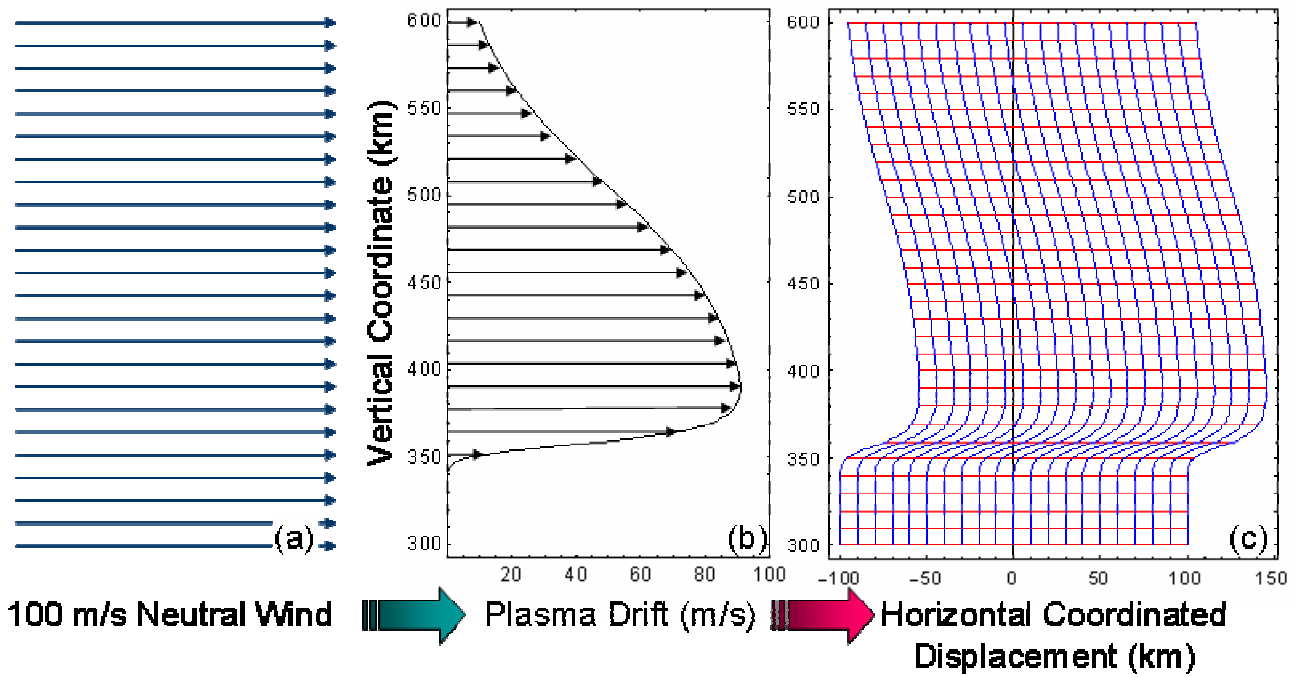


Figure 16. Horizontal coordinate distortion by wind induced plasma shear flow after 500 seconds of plasma motion.

The rising bubble will be caught in the sheared plasma flow to provide a tilt to the bubble. To model this tilt, the quasi-analytic transport model will be modified assuming that the bubble follows a trajectory that is a combination of the vertical rise velocity V_{y0} and the horizontal shear velocity given by (52). The equations for the trajectory of the center (x_c, y_c) of the bubble is

$$\frac{\partial y_c}{\partial t} = V_{y0} \text{ and } \frac{\partial x_c}{\partial t} = V_{xs}(y_c) \quad (57)$$

Assuming that the bubble starts to form at the initial location $(x, y) = (0, y_{c0})$, then the solution of (57) becomes

$$y_c = y_{c0} + V_{y0}t \text{ and } x_c = \int_0^t V_{sx}(y_{c0} + V_{y0}t') dt' \quad (58)$$

In normalized coordinates this solution for the center trajectory of the bubble becomes

$$\hat{y}_c = \hat{t} \quad \text{and} \quad \hat{x}_c = \int_0^{\hat{t}} \hat{V}_{xs}(\hat{\tau}) d\hat{\tau} \quad (59)$$

where distance is normalized by r_0 , velocities are normalized by V_{y0} and time is normalized by r_0/V_{y0} as before.

The simple coordinate map (57) neglects horizontal flow from internal polarization of the bubble. This flow is the result of vertical polarization fields generated by polarization of the bubble structure by the neutral wind. This process has been described in Section II except that, along with vertical gravitational acceleration, the horizontal neutral wind induces an electric potential that causes horizontal motion of the bubble center. From (6), the vector electric field from these forces is

$$\mathbf{E}_0 + \left(\mathbf{U} + \frac{\mathbf{g}}{V_{in}}\right) \times \mathbf{B} \equiv -\mathbf{E}_T \quad (60)$$

The horizontal neutral wind in the rest frame of the plasma bubble is $U_x - V_{x0}$ where V_{x0} is the horizontal velocity of the center of the bubble. The electric field associated with this neutral wind in this frame is

$$E_{Ty} \hat{y} \equiv (U_x - V_{x0}) B_0 \hat{y} \quad (61)$$

by the definition in (60). In the rest frame of the plasma, the relative velocity of the electric potential at altitude $y = y_c$,

$$V_{xR}(y_c) = \frac{E_{Ty}}{B_0} = -\frac{1}{B_0} \frac{\partial \Phi_1}{\partial y} \quad (62)$$

where Φ_1 is the potential from internal polarization.

The response of the plasma to this drive field is dependent on the physical structure of the bubble. For the tilted bubble model with internal polarization, a single parameter scaling of the ambient drifts is used. The horizontal drift velocity of the bubble center is assumed to have the form

$$V_{x0}(y) = (1 - a_y) V_{xS} = V_{xS} + V_{xR} \quad \text{with} \quad V_{xR} = -a_y V_{xS} \quad (63)$$

where a_y is a constant analogous to a_x used in the previous section to determine the bubble rise rate from gravity. The parameter a_y determines the bubble velocity in a rest frame of the background plasma.

The wind and plasma drift profiles in Figure 15 illustrate this polarization effect. Figure 15b shows that, near the peak, the relative wind in the plasma rest frame is about 10% of the total plasma drift. The parameter a_y controls the relative velocity of the bubble in the background plasma. If $a_y = 0$, the bubble drifts with the background plasma as if there were no internal polarization of the bubble. If $a_y = 1$, the background horizontal

Quasi-Analytic Models for Density Bubbles and Plasma Clouds in the Equatorial Ionosphere

plasma drift cancels the wind-induced relative motion produced by the polarization fields inside the bubble giving $V_{x0} = 0$ and $V_{xR} = -V_{xS}$. In normalized coordinates (63) becomes

$$\hat{V}_{x0} = \frac{V_{x0}}{V_{y0}} = (1 - a_y) \hat{V}_{xS} = \hat{V}_{xS} + \hat{V}_{xR} . \quad (64)$$

Using the definition of

$$a_y = -V_{xR}/V_{xS} \quad (65)$$

where V_{xR} is the measured bubble velocity relative to the background plasma drive V_{xS} .

The technique for bubble modeling is based on the motion of the analytic electric potential along a trajectory. The tilted bubble rises along the path defined by the velocity $\mathbf{V}_0 = V_{x0}\hat{\mathbf{x}} + V_{y0}\hat{\mathbf{y}}$. With both background drift and internal plasma motion, the dynamics of the center of the plasma bubble potential are given by

$$\frac{\partial y_c}{\partial t} = V_{y0} \quad \text{and} \quad \frac{\partial x_c}{\partial t} = V_{x0} = (1 - a_y)V_{xS} \quad (66)$$

with the initial conditions $[x_c(0), y_c(0)] = [0, y_{c0}]$.

For the tilted bubble model, the internal horizontal and vertical electric fields are considered along with of the overall motion of the background plasma. With the internal field assumption, the analytical potential function becomes

$$\begin{aligned} \Phi(x, y, t) &= \Phi_0(y) + \Phi_1(x - x_c, y - y_{c0} - V_{y0}t, 0) \\ &= \Phi_0(y) + B_0 \frac{[x - x_c(t)] V_{y0} - [y - y_{c0} - V_{y0}t] V_{xR} (y_{c0} + V_{y0}t)}{1 + \left[\left(\frac{x - x_c(t)}{r_0} \right)^2 + \left(\frac{y - y_{c0} - V_{y0}t}{r_0} \right)^2 \right]^{b/2}} \end{aligned} \quad (67)$$

which is identical to (39) with Φ_0 , V_{xR} and x_c equal to zero. The induced plasma bubble velocity in the horizontal direction is

$$V_{x0} = -\frac{1}{B_0} \frac{\partial \Phi}{\partial y} = V_{xS} + V_{xR} \quad (68)$$

at the position $x = x_c(t)$ and $y = y_{c0} + V_{y0}t$. The added variables tilt the electric potential off vertical so that the head of the bubble can flow against the ambient drift of the background plasma.

The coordinate shift $x_p = x - x_c(t)$ and $y_p = y - y_{c0} - V_{y0}t$ translates the potential into the reference frame of the bubble center with the result

$$\Phi(x, y, t) = \Phi_0(y) + B_0 \frac{x_p V_{y0} - y_p V_{xR}(y_{c0} + V_{y0}t)}{1 + (r_p/r_0)^b} \quad (69)$$

where $r_p^2 = x_p^2 + y_p^2$.

The potential function given by (65) is substituted into the Lagrangean transport equations

$$\frac{\partial x(x_0, y_0, t)}{\partial t} = -\frac{1}{B_0} \frac{\partial \Phi(x, y, t)}{\partial y} \quad \text{and} \quad \frac{\partial y(x_0, y_0, t)}{\partial t} = \frac{1}{B_0} \frac{\partial \Phi(x, y, t)}{\partial x} \quad (70)$$

The resulting coordinate mapping equations for the rising potential in sheared plasma flow is

$$\begin{aligned} \frac{\partial x_c}{\partial t} &= V_{x0}(y_c) = V_{x0}(y_{c0} + V_{y0}t) \\ \frac{\partial x}{\partial t} &= \frac{b r_p^{b-2} r_0^{-b} y_p [x_p V_{y0} - y_p V_{xR}(y_{c0} + V_{y0}t)] + [1 + r_p^b r_0^{-b}] V_{xR}(y_{c0} + V_{y0}t)}{(1 + r_p^b r_0^{-b})^2} + V_{xS}(y) \\ \frac{\partial y}{\partial t} &= \frac{V_{y0} [1 + r_p^b r_0^{-b}] - b r_p^{b-2} r_0^{-b} x_p [x_p V_{y0} - y_p V_{xR}(y_{c0} + V_{y0}t)]}{(1 + r_p^b r_0^{-b})^2} \end{aligned} \quad (71)$$

incorporating both internal and external forces on the bubble.

In normalized coordinates, the transport equations become

$$\begin{aligned} \frac{\partial \hat{x}_c}{\partial \hat{t}} &= V_{x0}(\hat{y}_c), \quad \hat{y}_c = \hat{t}, \\ \frac{\partial \hat{x}}{\partial \hat{t}} &= \frac{b \hat{r}_p^{b-2} \hat{y} [\hat{x} - \hat{V}_{sR}(\hat{y}_c) \hat{y}] + [1 + \hat{r}_p^b] \hat{V}_{sR}(\hat{y}_c)}{[1 + \hat{r}_p^b]^2} + \hat{V}_{xS}(\hat{y}) \\ \frac{\partial \hat{y}}{\partial \hat{t}} &= \frac{1 + \hat{r}_p^b - b \hat{r}_p^{b-2} \hat{x} [\hat{x} - \hat{V}_{sR}(\hat{y}_c) \hat{y}]}{[1 + \hat{r}_p^b]^2} \end{aligned} \quad (72)$$

where once again distance is normalized by r_0 , velocity is normalized by V_{y0} , and time is normalized by the quantity r_0/V_{y0} . The velocity functions are all related to the normalized plasma shear by the parameter a_y with $V_{x0}(\hat{y})/(1 - a_y) = -\hat{V}_{xR}(\hat{y})/a_y = \hat{V}_{xS}(\hat{y})$.

Before computing the coordinate mapping, the trajectory of the center of the potential function (x_c, y_c) is found by solving the first ordinary differential equation in (71) or (72). For this calculation and all the follow, the shear velocity shown in Figure 16 was used in (66) with a several values of a_y . Figure 17 illustrates the model results for the motion of bubble center as a function of the parameter a_y . With $a_y = 0$ the potential will rise and drift east reaching a maximum distance on the topside where the wind induced drift vanishes. As the parameter a_y is increased toward unity, the internal polarization of the bubble inhibits its horizontal motion in the background plasma flow.

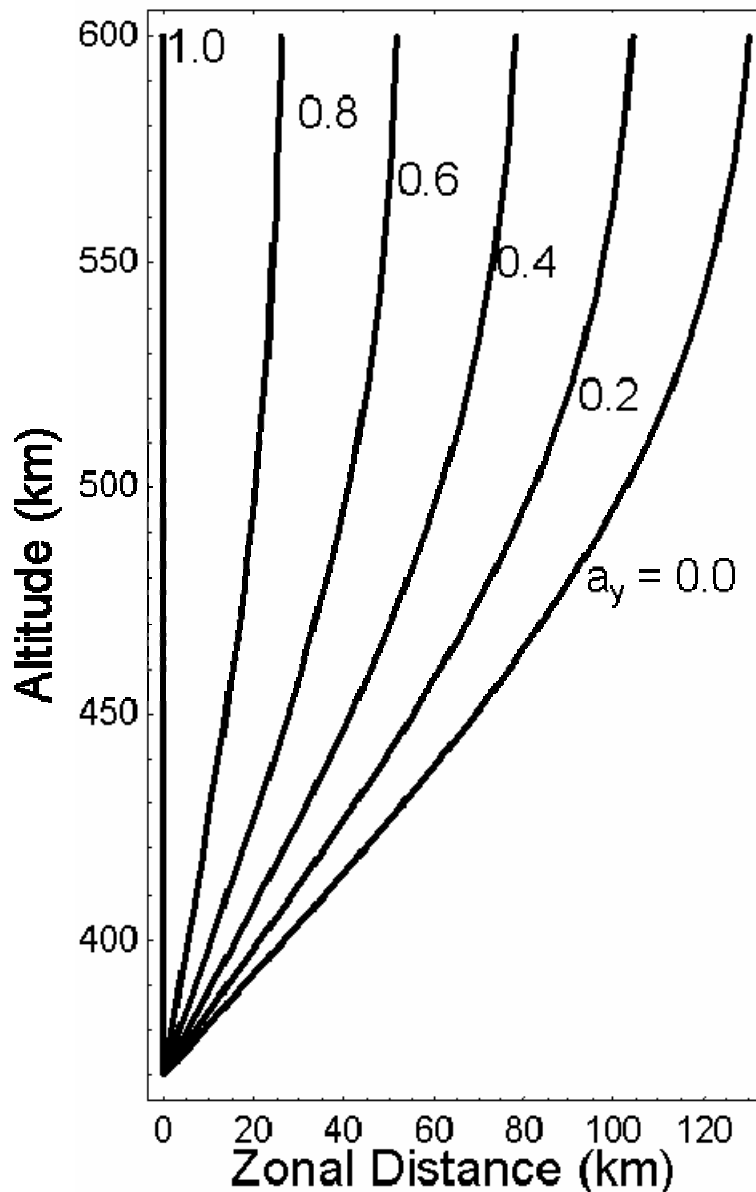


Figure 17. Curves of the trajectory for the analytic potential function used to create the equatorial bubble. With parameter $a_y = 0$, the internal polarization of the bubble is neglected and the potential function is transported by the full action of the plasma shear. As a_y is increased, the zonal motion of the center of the bubble potential is reduced. With $a_y = 1$, the internal polarization at the head of the bubble completely cancels the plasma drift of the ambient layer.

To illustrate the results from these coordinate-mapping equations, the parameter a_y is set to one-tenth so the potential function moves horizontally with the ambient plasma flow at each altitude and is slightly retarded by internal polarization. When $a_y = 0.1$, then $V_{xR}(y) = V_{xS}/10$, $V_{x0} = 9 V_{xS}/10$. The initial conditions for the coordinate map are $[\hat{x}_c(0), \hat{x}(0), \hat{y}(0)] = [0, \hat{x}_0, \hat{y}_0]$ at $\hat{t} = 0$. All of the results are displayed in normalized

coordinates. The normalization parameters $r_0 = 30$ km, and $v_{y0} = 100$ m/s can be used to translate the solutions back to physical space. The bubble moves with the vertical rise velocity from internal electric fields set up by gravity. By setting the internal polarization parameter a_y nearly to zero, the horizontal motion is primarily with the background plasma but there is a small retardation from the internal fields. The shear function was put into normalized form from the physics coordinates using the definition $\hat{y} = (y - y_{c0})/r_0$ where $y_{c0} = 370$ km. With the parameter $b = 4$, the ordinary differential equations given in (67) are integrated in time to yield the quasi-analytic solutions for the Lagrangean coordinate distortions shown in Figure 18. The center of the potential function as derived from the first equation in (72) is shown by the green curve in each figure. The plume structure below the top of the bubble becomes caught up in the ambient flow to form a backwards “C”. The successive images in Figure 18 are normalized shown for normalized times of 2, 4, and 6. Using the normalization factor $r_0/V_{y0} = 300$ seconds, the absolute times for the tilted bubble coordinate maps are (a) 600, (b) 1200, and (c) 1800 seconds.

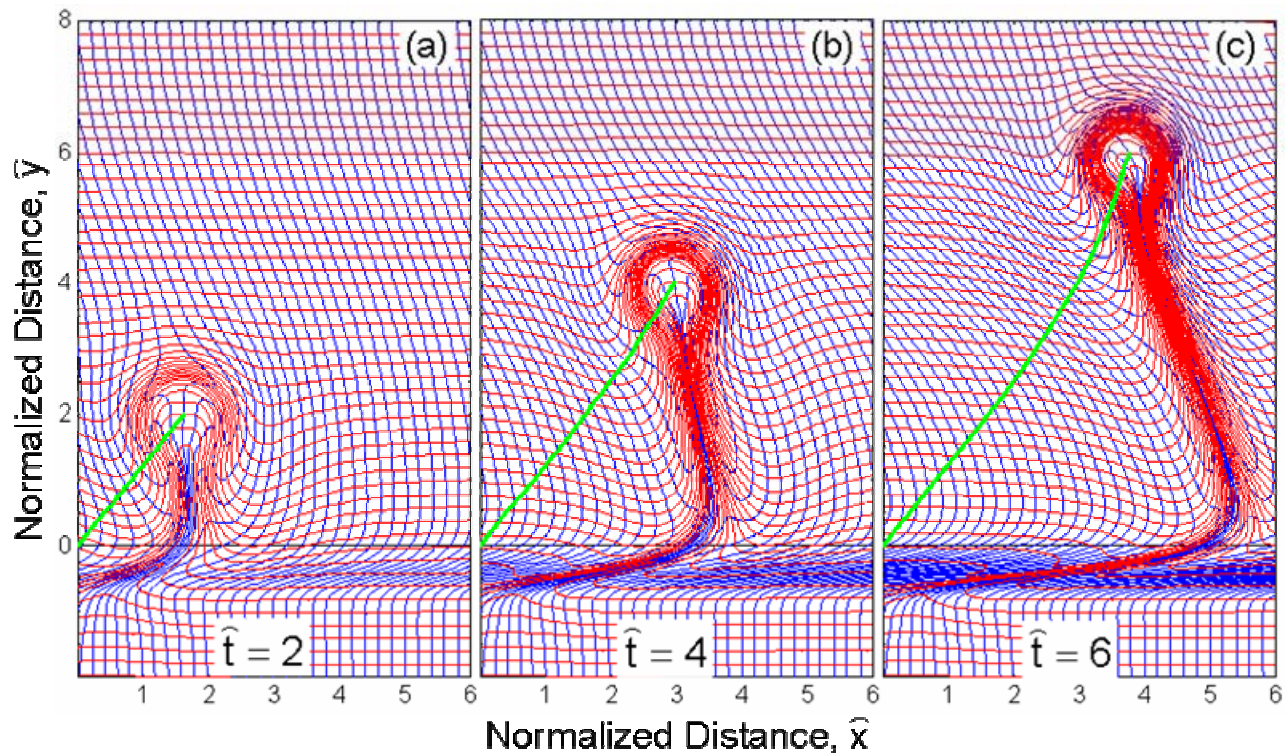


Figure 18 Coordinate map for distortions from a rising ($b = 4$) bubble in a sheared background plasma flow. The green line shows the trajectory of the center of the bubble with $a_y = 0.1$. The plume becomes curved as it is caught in the ambient plasma flow.

The coordinate transform equations in (72) yield the normalized, destination coordinates $[\hat{x}(\hat{t}), \hat{y}(\hat{t})]$ from the given initial coordinates $[\hat{x}_0, \hat{y}_0]$. To determine a mapped density at a given location, the time-inverse transformation to determine the initial coordinates for a coordinate cell that is transported to a given location. This inverse transform has already been discussed in the previous section for bubbles with out tilts. This inverse map are obtained by replacing t with $-t$ in (72). The center of the potential function starts at location $\hat{x}_0 = x_c(\hat{t}_1)$ and $\hat{y}_0 = \hat{t}_1$.

Quasi-Analytic Models for Density Bubbles and Plasma Clouds in the Equatorial Ionosphere

The solution for the inverse coordinate transform proceeds in two steps. First, the initial equation in (72) is solved to yield the function $x_c(t)$ for the horizontal displacement of the bubble potential function. Next, the system given by (68) is integrated as the potential follows a trajectory $[\hat{x}_c(\hat{t}), \hat{y}_c(\hat{t})]$ to end at the origin of the normalized coordinate system where $\hat{x}_0 = 0$ and $\hat{y}_0 = 0$. The curves in Figure 17 show the $[\hat{x}_c(\hat{t}), \hat{y}_c(\hat{t})]$ trajectories as a function of the internal polarization factor a_y . As previously discussed with (47), the inverse coordinate map equations are integrated from $\hat{t} = -\hat{t}_1$ to $\hat{t} = 0$. The initial conditions for (72) are

$$\hat{x}_0(-t_1) = \hat{x}_1 \text{ and } \hat{y}_0(-t_1) = \hat{y}_1 \quad (73)$$

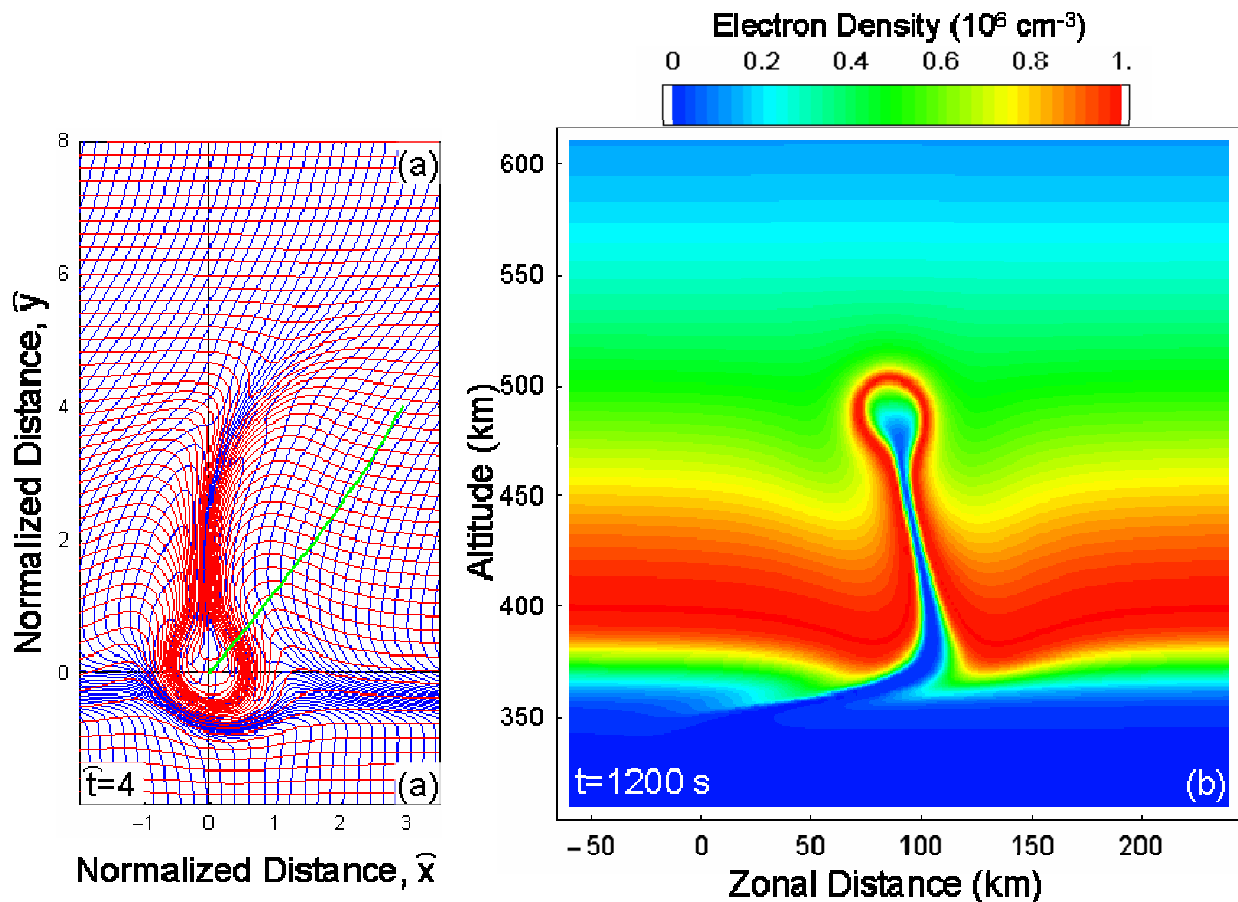


Figure 19 Computed examples of (a) inverse coordinate map at $\hat{t} = 4$ and (b) corresponding ionospheric bubble densities at $t = 1200$ seconds for the electric potential moving through a sheared plasma with small internal polarization ($a_y = 0.1$). The parameters for the simulation are identical to those used to generate Figure 12 which can be used for comparison to illustrate the effects of the zonal wind on tilting the bubble.

The inverse coordinate map for the rising bubble the sheared plasma flow is illustrated in Figure 19a in normalized coordinates at the normalized time $\hat{t} = 4$. This coordinate map presents the origin of the plasma

cells that have been transported to the west by the wind induced horizontal transport and the gravity induced vertical transport. The parameter a_y is set to zero so the horizontal transport by internal polarization of the equatorial bubble is neglected.

When the inverse coordinate map is applied to the background plasma layer, the electron densities are to form the tilted plume structure in Figure 19b. The depletion at the center of the bubble is the result of incompressible convection from the bottom to the topside of the layer. In this model, the reduced density channel extends over 100 km down through the layer to the bottom of the F-region. The absolute spatial dimensions are derived using a scale length $r_0 = 30$ km and a base height $y_{c0} = 370$ km. As with Figure 17, the time normalization factor is 300 seconds.

6.0 NORMALIZATION IN THE ANALYTIC MODELS OF THE DISTURBED IONOSPHERE

In the simulations of the previous three sections, the electric potential was fixed as it rose through the plasma layer forming bubble structures. The next step in the quasi-analytic modeling is to adjust the model parameters to make the computed electron density consistent with the electric potential. The appropriate values of both parameters (a_x and b) are obtained by comparing the analytic solutions given in (19) with the quasi-analytic solutions obtained by compressing the F-layer coordinates using (47) for an untilted bubble or (71) for a plume with internal polarization and plasma shear flow.

The vertical bubble motion comes from polarization of the horizontal density gradients. The horizontal Pedersen conductivity from (21b) through the center of the electric potential is given by

$$\Sigma_p^{(1)}(\bar{x}, 0) = \exp \left\{ \frac{a(1+m)}{A_1} \left[2 \tan^{-1} \left(\frac{B_1 - 2|\bar{x}|^b}{A_1} \right) - \text{sign}(a) \pi \right] \right\} \frac{C_0 (1 + |\bar{x}|^b)^2}{1 - a - B_1 |\bar{x}|^b + \bar{x}^{2b}} \quad (74)$$

where $A_1 = \sqrt{-a[4b + a(b-1)^2]}$ and $B_1 = -a(b-1) - 2$ and $|\bar{x}| = \sqrt{\bar{x}^2}$. Assume that the electron density at the equator is directly proportional to the integrated Pedersen conductivity. In absolute coordinates, the analytic model for the horizontal electron density profile through the center of the bubble is

$$N_e(x_p, y_c(t)) = \exp \left\{ \frac{a(1+m)}{A_1} \left[2 \tan^{-1} \left(\frac{B_1 - 2|x_p/R_1|^b}{A_1} \right) - \text{sign}(a) \pi \right] \right\} \frac{C_1 (1 + |x_p/R_1|^b)^2}{1 - a - B_1 |x_p/R_1|^b + |x_p/R_1|^{2b}} \quad (71)$$

where $x_p = x - x_c(t)$ is the horizontal distance relative to the center of the potential function and $\{x_c(t), y_c(t)\}$ is the location of this center. The corresponding electric potential is

$$\Phi(x, y, t) = B_0 \frac{[x - x_c(t)] V_{y0}(t) + [y - y_c(t)] V_{xR}(y_c(t))}{1 + \left[\left(\frac{x - x_c(t)}{R_1(t)} \right)^2 + \left(\frac{y - y_c(t)}{R_1(t)} \right)^2 \right]^{b(t)/2}} \quad (75)$$

where $a_x(t)$, $b(t)$, $R_1(t)$, and $C_1(t)$ are parameters that will be allowed to vary with time as the bubble evolves.

Quasi-Analytic Models for Density Bubbles and Plasma Clouds in the Equatorial Ionosphere

The bubble rise velocity $V_{y0}(t) = \frac{a_x(t) E_{Tx}}{B_0}$ and the bubble retardation velocity $V_{xR} = a_y V_{xS}$ have been defined in the previous sections. The electric potential follows a trajectory given by

$$\begin{aligned} \frac{\partial x_c}{\partial t} &= V_{x0}(y_c) = (1 - a_y) V_{xS}(y_c) \\ \frac{\partial y_c}{\partial t} &= V_{y0}(t) = \frac{a_x(t) E_{Tx}}{B_0} \end{aligned} \quad (76)$$

With this trajectory, the Lagrangean coordinate map

$$\frac{\partial x(x_0, y_0, t)}{\partial t} = -\frac{1}{B_0} \frac{\partial \Phi(x, y, t)}{\partial y} + V_{xS}(y) \quad \text{and} \quad \frac{\partial y(x_0, y_0, t)}{\partial t} = \frac{1}{B_0} \frac{\partial \Phi(x, y, t)}{\partial x} \quad (77)$$

is again used to determine the distortion of the plasma layer. The normalization procedure fits the function given by (73) to the densities determined using the Lagrangean transport given by (77) as applied to the stratified plasma profile.

Tests of the normalization procedure has demonstrated that the numerical value for the temporal normalization constant $a_x E_{Tx}/(B_0 r_0)$ is equal to approximately 70% of the calculated growth rate $\gamma = (-E_{Tx}/B_0)/L_N$ of the instability so that the parameter ratio $-r_0/a_x \approx L_N/0.7$. The recommended procedure for providing reasonable models of equatorial bubbles is to first choose a scale length r_0 that matches the dimension of the “seed” needed to produce the bubble. Second, select the potential amplitude using the simple expression $a_x \approx -0.7 r_0/L_N$ where $L_N = Ne(y)/\frac{\partial Ne(y)}{\partial y}$ is the initial scale length of the bottomside of the background ionosphere.

7.0 CONCLUSIONS

At this point, all the steps outlined in Figure 1b have been completed and the densities for the ionospheric bubble can be computed with relative ease. The only numerical computation is a solution of the ordinary differential equations (72) which are applied to the model of the unperturbed ionosphere. Physics based simulations of equatorial plumes can be computed with relatively high speed using a simple form for the electric potential that has 4 parameters that are adjusted based on numerical model fits to the electron density at each time step. This fit procedure occurs only at the altitude of the center of the bubble potential function. The spatial and temporal scales for the simulations are all normalized with a constant r_0 . The Lagrangean Map can be applied to a wide variety of ionospheres. This flexibility allows the generation of a wide range equatorial bubbles without complete re-computation of the densities. The examples have illustrated the integrated Pedersen conductivities plotted at the equatorial plane. The densities along the magnetic field lines may be obtained by solving for one-dimensional field-aligned diffusion of the plasma as they are transported by the bubble electric fields.

The formulas described here provide the electron densities that can be used for a wide range of ionospheric applications including ray path propagation, diffraction screen formation, radar and navigation error

estimation, and communications systems effects prediction. The major use of this model is to predict observations from new sensors launched into space. The results of this model have been predictions of the signature of equatorial bubbles on GPS occultation receivers in low-earth orbit (LEO) [3] and the phase and amplitude scintillations that would be recorded from ground-to-space propagation from UHF beacons to LEO satellites [4]. A secondary use of this formulation is to provide incite into the formation of equatorial bubbles. The analytic formulation has shown that (1) a continuous range of electron density structures will yield the same electric potential distribution, and (2) the electric potential that contributes to the evolution of the bubble is concentrated near the head. Future research using this technique will examine the triggering of bubbles using initial distributions shown in Figure 4 and bifurcations of bubbles where the single potential function is analytically split into a pair of potentials.

APPENDIX A. NUMERICAL SOLUTION OF THE POTENTIAL EQUATION USING A DIRECT SOLVER.

Numerical solutions are required when conditions of simplified geometries or uniform flows yield a complicated, nonlinear partial differential equation for the electric potential. In Cartesian coordinates, the non-separable elliptic equation that describes the electric potential is given by (7) and is repeated in equivalent form here

$$\Sigma_p \frac{\partial^2 \hat{\Phi}}{\partial \bar{x}^2} + \frac{\partial \Sigma_p}{\partial \bar{x}} \frac{\partial \hat{\Phi}}{\partial \bar{x}} + \Sigma_p \frac{\partial^2 \hat{\Phi}}{\partial \bar{y}^2} + \frac{\partial \Sigma_p}{\partial \bar{y}} \frac{\partial \hat{\Phi}}{\partial \bar{y}} = \frac{\partial \Sigma_p}{\partial \bar{x}} \quad (A1)$$

The conductivity function $\Sigma_p(\bar{x}, \bar{y})$ is known and the potential function $\hat{\Phi}(\bar{x}, \bar{y})$ is found as a numerical solution to the equation (A1).

This equation is converted into a set of linear equations using the usual finite difference approximations to the derivatives given by

$$\begin{aligned} \frac{\partial^2 \hat{\Phi}}{\partial \bar{x}^2} &\rightarrow \frac{\hat{\Phi}_{i+1,j} - 2\hat{\Phi}_{i,j} + \hat{\Phi}_{i-1,j}}{\Delta \bar{x}^2} \\ \frac{\partial^2 \hat{\Phi}}{\partial \bar{y}^2} &\rightarrow \frac{\hat{\Phi}_{i,j+1} - 2\hat{\Phi}_{i,j} + \hat{\Phi}_{i,j-1}}{\Delta \bar{y}^2} \\ \frac{\partial \hat{\Phi}}{\partial \bar{x}} &\rightarrow \frac{\hat{\Phi}_{i+1,j} - \hat{\Phi}_{i-1,j}}{2\Delta \bar{x}} \\ \frac{\partial \hat{\Phi}}{\partial \bar{y}} &\rightarrow \frac{\hat{\Phi}_{i,j+1} - \hat{\Phi}_{i,j-1}}{2\Delta \bar{y}} \end{aligned} \quad (A2)$$

The Pedersen conductivity is sampled in the uniform solution grid spaced by Δx and Δy to form the array variables $\Sigma_{p,i,j}$ with $(i=1,2, \dots, M)$ and $(j=1, 2, \dots, N)$. To complete the solution, boundary conditions of periodic, fixed/Dirichlet, derivative/Neumann or mixed form are provided.

Quasi-Analytic Models for Density Bubbles and Plasma Clouds in the Equatorial Ionosphere

The unknowns $\hat{\Phi}_{i,j}$ for $(i=1,2, \dots, M)$ and $(j=1, 2, \dots, N)$ are grouped into linear arrays given by

$$\mathbf{X}_j = [\Phi_{1,j} \dots \Phi_{M,j}] \quad (\text{A3})$$

The resulting linear system can be written as an extended tri-diagonal matrix

$$\begin{bmatrix} \mathbf{B}_1 & \mathbf{C}_1 & \mathbf{0} & \dots & \mathbf{0} & \mathbf{0} & \mathbf{A}_1 \\ \mathbf{A}_2 & \mathbf{B}_2 & \mathbf{C}_2 & \dots & \mathbf{0} & \mathbf{0} & \mathbf{0} \\ \mathbf{0} & \mathbf{A}_3 & \mathbf{B}_3 & \dots & \mathbf{0} & \mathbf{0} & \mathbf{0} \\ \vdots & \vdots & \vdots & \ddots & \vdots & \vdots & \vdots \\ \mathbf{0} & \mathbf{0} & \mathbf{0} & \dots & \mathbf{B}_{N-2} & \mathbf{C}_{N-2} & \mathbf{0} \\ \mathbf{0} & \mathbf{0} & \mathbf{0} & \dots & \mathbf{A}_{N-1} & \mathbf{B}_{N-1} & \mathbf{C}_{N-1} \\ \mathbf{D}_1 & \mathbf{D}_2 & \mathbf{D}_3 & \dots & \mathbf{D}_{N-2} & \mathbf{D}_{N-1} & \mathbf{D}_N \end{bmatrix} \begin{bmatrix} \mathbf{X}_1 \\ \mathbf{X}_2 \\ \mathbf{X}_3 \\ \vdots \\ \mathbf{X}_{N-2} \\ \mathbf{X}_{N-1} \\ \mathbf{X}_N \end{bmatrix} = \begin{bmatrix} \mathbf{Y}_1 \\ \mathbf{Y}_2 \\ \mathbf{Y}_3 \\ \vdots \\ \mathbf{Y}_{N-2} \\ \mathbf{Y}_{N-1} \\ \mathbf{Y}_N \end{bmatrix} \quad (\text{A5})$$

where the $M \times M$ block matrices \mathbf{A}_j , \mathbf{B}_j , and \mathbf{C}_j are functions of the finite difference parameters and the Pedersen conductivity samples $\Sigma_{p,i,j}$. The matrices \mathbf{A}_1 and \mathbf{D}_1 are needed for periodic boundaries in the y -direction. The string of matrices $[\mathbf{D}_1, \mathbf{D}_2, \mathbf{D}_3, \dots, \mathbf{D}_{N-1}, \mathbf{D}_N]$ allow inclusion of an additional condition on the potential such as

$$\iint \hat{\Phi}(\bar{x}, \bar{y}) d\bar{x} d\bar{y} = 0. \quad (\text{A6})$$

This condition arises when the addition of a constant to a solution also yields solution. The nonuniqueness occurs if the boundary conditions are completely periodic and/or specified by constant derivatives (i.e., Neumann). With these types of boundary conditions, (A6) prevents the square matrix in (A5) from being singular and a numerical solution can be obtained. Finally, the right side of (A1) and boundary conditions are contained in the linear arrays \mathbf{Y}_j .

The algorithm for solving (A5) is a generalization of the Thomas Algorithm for scalar tridiagonal systems [5]. Initialize with new matrix variables

$$\mathbf{a}_1 = \mathbf{B}_1^{-1}, \mathbf{S}_1 = \mathbf{a}_1 \cdot \mathbf{Y}_1, \mathbf{a}_2 = \mathbf{a}_1 \cdot \mathbf{C}_1, \mathbf{b}_1 = -\mathbf{a}_1 \cdot \mathbf{A}_1 \quad (\text{A7})$$

Continue with the equations

$$\mathbf{a}_i = \mathbf{a}_{i-1} \cdot \mathbf{C}_{i-1}, \mathbf{a}_i = [\mathbf{B}_i - \mathbf{A}_i \cdot \mathbf{a}_i]^{-1}, \mathbf{S}_i = \mathbf{a}_i \cdot [\mathbf{Y}_i - \mathbf{A}_i \mathbf{S}_{i-1}], \mathbf{b}_i = -\mathbf{a}_i \cdot \mathbf{A}_{i-1} \cdot \mathbf{b}_{i-1} \quad (\text{A8})$$

for the index in the range $i = 2, \dots, N-1$. The next operations define a new set of variables starting with $\mathbf{S}'_N = \mathbf{0}$, $\mathbf{b}'_N = \mathbf{I}$, where \mathbf{I} is the $M \times M$ identity matrix, and continue with

$$\mathbf{S}'_{N-i} = \mathbf{S}_{N-i} - \mathbf{a}_{N-i+1} \mathbf{S}'_{N-i+1}, \mathbf{b}'_{N-i} = \mathbf{b}_{N-i} - \mathbf{a}_{N-i+1} \mathbf{b}'_{N-i+1} \quad (\text{A9})$$

for the index “i” in the range $i = 1, \dots, N - 1$. The solution for $j = N$ is given by

$$\mathbf{X}_N = \left[\sum_{i=1}^N \mathbf{D}_i \cdot \mathbf{b}'_i \right]^{-1} \cdot \left[\mathbf{Y}_N - \sum_{i=1}^N \mathbf{D}_i \cdot \mathbf{S}'_i \right]. \quad (\text{A10})$$

The remaining solution vectors are found from

$$\mathbf{X}_i = \mathbf{S}'_i + \mathbf{b}'_i \cdot \mathbf{X}_N \quad (\text{A11})$$

where the index “i” is given by the range $i = 1, \dots, N - 1$. This algorithm was used to provide the numerical potential solutions illustrated in Figure 5 and the data given in Tables II and III.

Acknowledgments. This research was sponsored at the Naval Research Laboratory by the Office of Naval Research. The author thanks Dr. Steven T. Zalesak for critical comments on this paper.

8.0 REFERENCES

- [1] Bernhardt, P.A. and J.U. Brackbill, "Solution of Elliptic Equations Using Fast Poisson Solvers," **J. Comp. Phys.**, 53, 382, 1984.
- [2] Bernhardt, P.A., Cross-B convection of artificial created, negative-ion clouds and plasma depressions: low-speed flows, **J. Geophys. Res.**, **93**, 8696-8704, 1988.
- [3] Bernhardt, P.A., Eye on the Ionosphere: Ionospheric Profiling by GPS Receiver Occultations, Taking Advantage of Existing Earth-Based Infrastructure, **GPS Solutions**, 9(1), 174-177, 2005
- [4] Bernhardt, P.A. and C.L. Siefring, I.J. Galysh, T.F. Rodillo, D.E. Koch, T.L. MacDonald, M.R. Wilkens, G.P. Landis, Ionospheric Applications of the Scintillation and Tomography Receiver in Space (CITRIS) used with the DORIS Radio Beacon Network, **J. Geodesy (in press)**, 2006
- [5] Dahlquist, G., A Bjorck, N. Anderson, Numerical Methods, Prentice-Hall, 1974.
- [6] Kelley, M. C., **The Earth's Ionosphere**, Academic Press, 1989
- [7] Richtmyer, R.D., and K.W. Morton, **Difference Methods for Initial-Value Problems**, Interscience, New York, 1967.
- [8] Zalesak, S.T., S.L. Ossakow, P.K. Chaturvedi, Non-linear equatorial spread-F – The effect of neutral winds and background Pedersen conductivity, **J. Geophys. Res.**, **87**, 151-166, 1982.
- [9] Zalesak, S. T., Fully multidimensional flux corrected transport algorithms for fluids, **J. Comput. Phys.**, 31, 355, 1979.

**Quasi-Analytic Models for Density Bubbles
and Plasma Clouds in the Equatorial Ionosphere**

